UNCLASSIFIED
~~RESTRICTED~~

Copy No. 47 ~~326~~
RM No. A7D11

CLASSIFICATION CHANGED

Copy 2

UNCLASSIFIED

NACA

authority of H. L. Dryden 6-5-53
per NACA Release form # 1428
By HGR, 7-15-53.

RESEARCH MEMORANDUM

MEASUREMENTS OF THE DAMPING IN ROLL OF LARGE-SCALE SWEPT-FORWARD AND SWEPT-BACK WINGS

By

Lynn W. Hunton and Joseph K. Dew

Ames Aeronautical Laboratory
Moffett Field, Calif.

NATIONAL ADVISORY COMMITTEE FOR AERONAUTICS

WASHINGTON

July 30, 1947

~~RESTRICTED~~

UNCLASSIFIED

NATIONAL ADVISORY COMMITTEE FOR AERONAUTICS

RESEARCH MEMORANDUM

Measurements of the Damping in Roll of Large-Scale Swept-Forward and Swept-Back Wings

By Lynn W. Hunton and Joseph K. Dew

SUMMARY

Wind-tunnel tests of five large-scale tapered wings which had angles of sweep of 0°, $\pm 30^{\circ}$, and $\pm 45^{\circ}$ have been conducted to determine the effects of both scale and sweep on the damping-in-roll parameter C_{l_p}. Rolling moment and pressure distribution were measured for each plain wing while in steady roll for an angle-of-attack range of -1° to 29°. The effects of both Reynolds number and deflection of partial-span split flaps were determined from less comprehensive tests. Several methods of predicting both the damping-in-roll and autorotational characteristics of the swept wings have been analyzed, and predicted results have been compared with the experimental data.

The variation of C_{l_p} with sweep at zero lift is shown to follow quite accurately the concepts of simple sweep theory, provided that corrections for aspect ratio based on the span perpendicular to the plane of symmetry are considered. It was found that the value of C_{l_p} for a swept wing at zero lift can be predicted within 6 percent by applying a correction for sweep to the damping derivative estimated from curves derived from lifting-surface theory for an unswept wing with the same aspect ratio, taper ratio, and section characteristics as those of the swept wing.

The damping in roll increased moderately with lift coefficient below the stall for all wings except the highly swept-forward wing, where a 104-percent increase was observed. Pressure-distribution data accounted for this phenomenon by indicating an increase of almost 100 percent in the section lift-curve slope at outboard portions of the wing.

The magnitude of the autorotational moment was found to be reduced by sweep and augmented by the deflection of partial-span split flaps. Predicted autorotational characteristics of the unswept and swept-forward wings as determined from Glauert's theory for autorotation are shown to be in good agreement with the experimental results; whereas for the swept-back wings the theory was found to be inapplicable.

INTRODUCTION

Knowledge of values of the damping-in-roll parameter C_{l_p} is of great importance in dynamics calculations involving rolling motion of an airplane. Little experimental data on C_{l_p} are available at the present time for either conventional or swept wings. As a result, estimated damping-in-roll characteristics have to be relied upon for dynamic stability calculations. The effects of variations in plan form involving aspect ratio and taper ratio on C_{l_p} for straight wings have in the past been analyzed theoretically by many authors. Usually they employed the early concepts of Glauert, who first used a Fourier series to express the circulation (reference 1), and Munk, who derived the induction factor for rolling moment (reference 2). Elementary aerodynamic considerations indicate that C_{l_p} would be greatly affected by sweep. The first-order effects of sweep on C_{l_p} have been predicted by theory and have been obtained experimentally by brief investigations made at very low Reynolds number.

In view of the limited amount of experimental and theoretical analysis at hand for highly swept wings, an investigation of large-scale swept-forward and swept-back wings was undertaken in the Ames 40- by 80-foot wind tunnel. Included in this swept-wing program were: (a) an evaluation and analysis of the static stability and control characteristics (reference 3); (b) a comparison of the span loading for swept wings as calculated by three theoretical methods with the experimentally measured span load distribution (reference 4); and (c) an investigation of the damping-in-roll characteristics reported herein.

The present investigation covered measurements of rolling moment together with pressure distribution for the swept wings in steady roll. The accuracy of various theories are evaluated by comparing the measured value of C_{l_p} for each swept wing with those computed by a method of Weissinger (reference 4) and by simple formulas which correct the C_{l_p} value of the unswept wing for sweep angle and aspect ratio. Values of C_{l_p} for the unswept wing were estimated by the methods of references 5 and 6.

SYMBOLS

The symbols used in this report are defined as follows:

C_L lift coefficient $\left(\frac{\text{lift}}{qS}\right)$

C_D drag coefficient $\left(\frac{\text{drag}}{qS}\right)$

C_l rolling-moment coefficient $\left(\frac{\text{rolling moment}}{q\ S\ b}\right)$

C_Y side-force coefficient $\left(\frac{\text{side force}}{q\ S}\right)$

C_{L_α} rate of change of lift coefficient with angle of attack, per radian

C_{l_β} rate of change of rolling-moment coefficient with angles of sideslip, per degree

C_{Y_β} rate of change of side-force coefficient with angle of sideslip, per degree

C_{l_p} damping-in-roll parameter; rate of change of rolling-moment coefficient with wing-tip helix angle $\left(\frac{\partial C_l}{\partial pb/2V}\right)$

c_l section lift coefficient $\left(\frac{\text{section lift}}{qc}\right)$

$pb/2V$ wing-tip helix angle, radians

$\frac{c_l c}{pb/2V}$ span-loading parameter in roll

α_u geometric angle of attack of root chord relative to tunnel center line, degrees

α true angle of attack of root chord relative to air stream, degrees

β angle of sideslip, degrees

Λ angle of sweep of quarter-chord line, degrees (Sweepback is positive and sweepforward is negative.)

A aspect ratio based on span $\left(\frac{b^2}{S}\right)$

A' aspect ratio based on length of quarter-chord line $\left(\frac{b^2}{S \cos^2\Lambda}\right)$

b wing span measured perpendicular to the plane of symmetry, feet

c chord length at any section of wing measured parallel to air stream, feet

c_t wing-tip chord, feet

c_r wing-root chord, feet

E'_{e_c} effective edge-velocity correction factor for rolling moment

p angular velocity in roll, radians per second

q free-stream dynamic pressure, pounds per square foot

R Reynolds number

S wing area, square feet

V free-stream velocity, feet per second

DESCRIPTION OF APPARATUS

The five large-scale tapered swept wings used in the investigation were the same wings used for the static tests and are fully described in reference 3. Composed primarily of a set of wing panels from an existing airplane, the wings were given the desired plan form and sweep (0°, 30°, and 45° sweepforward, 30° and 45°

sweepback) by the addition of individually fabricated tips and center sections. Plan-form drawings and geometric characteristics of the five wings are shown in figure 1. The airfoil sections for each of the swept wings were dictated by the sections of the wing panel (NACA 0015 at the inboard end of the panel and NACA 23009 at the outboard end). The right wing panel, tips, and center sections were equipped with 180 pressure orifices located at 8 spanwise stations. For the flap-deflected condition, partial-span split flaps were attached to the wings at an angle of 60°[1]. The flaps had a chord 20 percent of the wing chord, were tapered with the wing chord, and extended over the inboard 62.3 percent of the span for all wings. The condition of the wing surfaces, which had a normal amount of roughness caused by access hatches and flush rivets, was equivalent to that of present-day production airplanes.

The rolling-wing support stand shown in figure 2 was essentially an elevated steel platform on which was mounted a 1000-horsepower variable-speed induction drive motor, a geared reduction unit, and a 13-inch-diameter steel torque tube mounted in two self-alining bearings. The axis of rotation was at all times coincident with the center line of the tunnel. Each of the swept-wing center sections was slotted to fit over the end of the cantilevered torque tube, which provided a means of attachment and adjustment of the angle of attack from -1° to 29°.

Instrumentation for the tests consisted of equipment for measuring and recording continuously the rolling torque, wing position in the test section, and pressure distribution. A resistance-type torsion strain gage equipped with monel slip rings and carbon silver brushes (shown in figure 2(a)) was used in conjunction with a recording oscillograph to measure the rolling resistance of the wing. A time impulse at intervals of 1 second and the position of the wing at intervals of one-quarter cycle were recorded on the torque record, thus providing a check on the accuracy of an aircraft tachometer which was used to establish the rolling velocity. For the pressure measurements, recording manometers were installed in the wing center section. Power for operation and time impulse for synchronization with the torque record were supplied through a second set of slip rings also shown in figure 2(a). The two manometers contained a total of 90 pressure-recording cells, each of which was connected to a pair of pressure orifices located oppositely on the upper and lower surface in order to record directly the local differential pressure.

---

[1]All chords and spans used in this report were measured parallel and perpendicular, respectively, to the plane of symmetry. Flap angles were measured in a plane perpendicular to the flap hinge line.

TESTS AND REDUCTION OF DATA

For the determination of the damping characteristics of the wings, the torque variation was recorded continuously throughout a complete cycle in steady roll for each test condition. The data for a given condition were then reduced to the desired damping moment by integrating this torque variation for one cycle to obtain an average rolling moment due to roll.

As outlined in table I, tests were made at a dynamic pressure of 20 pounds per square foot ($R = 5.6 \times 10^6$ to 8.95×10^6 for the various wings based on the M.A.C.) for eight different angles of attack varying from -1° to 29° for each swept wing without flaps (hereafter referred to as a plain wing). Rolling-torque and pressure-distribution data were obtained at each attitude for wing-tip helix angles ranging from 0 to ±0.11 radian. In addition, damping-moment tests at the high-speed attitude of each wing were made at dynamic pressures of 60 and 120 pounds per square foot ($R = 9.3 \times 10^6$ and 12.5×10^6, respectively, for the unswept wing).

The tests of the wings with 60° partial-span split flaps (hereafter referred to as flapped wings) were run at a dynamic pressure of 20 pounds per square foot. Rolling-moment data were obtained at only the higher angles of attack (9° to 29°) for $pb/2V$ values ranging from 0 to 0.11 radian.

In order to present consistent rolling-moment data, the moments have been computed about an axis located similarly in each swept wing. All the data have been corrected and presented with reference to an axis of roll parallel to the air stream and located such that the quarter M.A.C. point of each wing panel was in pure roll (i.e., no sideslip velocity). The necessity for a correction arises from the fact that only at an angle of attack of 0° was the chord plane of each wing coincident with the actual axis of roll. The method of attachment of the wing to the torque tube required that the angle of attack be changed by pitching the wing about a point which varied for the several wings from 8 feet aft to 4 feet ahead of the quarter M.A.C. point. It is apparent that for these wings in steady roll at any angle of attack other than 0° a certain amount of sideslip velocity was introduced at the quarter M.A.C. point. A correction based on the rolling moment due to sideslip of each wing, equal to the increment of damping-in-roll parameter ΔC_{l_p} shown in table II, has been added algebraically to each measured rolling-moment coefficient. The values of dihedral effect C_{l_β} for each wing for these sideslip corrections were obtained from force tests reported in reference 3. A correction resulting from the side-force parameter C_{Y_β} was computed in a similar manner; it was found to be insignificant and therefore has been neglected.

The problem of tunnel-wall corrections was investigated to determine the effect of boundary interference on the static characteristics of the swept wings. The analysis indicated that the average tunnel-wall correction was nearly the same for any of the wings considered. Hence, approximate corrections based on the unswept plan form at the horizontal position in the test section have been applied to the angle of attack for each swept wing.

A second tunnel-wall correction which involved the boundary influence on the damping in roll was investigated. This analysis was complicated by the fact that the closed throat modified rectangular test section (outline of boundary may be noted in background of figure 2(c)) varied in width-to-height ratio with the rotational position of the wing. As an approximation, interference effects were determined for two positions of the wing (horizontal and vertical) with a resultant boundary width-to-height ratio of 2:1 and 1:2, respectively. It was assumed in both cases that the test section was rectangular and that the static induction effects of the wing at rest would closely approximate those of the wing in steady roll. In general, the method employed was that of infinite image systems where each image consisted of an infinite vortex sheet the intensity of which varied spanwise approximately as the antisymmetric wing-loading increment generated by the rolling wing. Computations of the induced effects on the downwash at four sections of the wing semispan showed that for the wing-horizontal configuration the boundary influence varied from a downwash at the downgoing tip of the wing to an upwash at the upgoing tip. Spanwise integration of the variation of induced angle of attack indicated that the measured damping moments were 2 percent low when the wing was near the horizontal position. For the case of the wing in the vertical position, where the induction effects varied from an upwash at the downgoing wing tip to a downwash at the upgoing tip, the damping measurements were 9 percent high. Since the value of this correction apparently oscillated between a supporting and a resisting moment, its effect can be minimized by determining the average rolling moment over a complete rolling cycle. This procedure would then involve a maximum over-all tunnel-wall influence of approximately 3 percent. The data reported herein were obtained by such averaging and the wall-interference correction has been neglected.

Tests of the torque tube in roll with the wing removed showed no measurable friction. The two self-alining bearings were subject to only 5 percent of their rated load carrying capacity when under the maximum test load condition.

RESULTS AND DISCUSSION

Damping-moment data for the five swept wings, both plain and flapped, are presented in figures 3 and 4, respectively, as variations of C_l with $pb/2V$. Values of C_{l_p}, as determined from the slopes of the curves of figure 3 at $pb/2V = 0$, are given in figure 5 as a function of α. Also shown in figure 5 are the corresponding lift curves taken from reference 3. The variations of C_{l_p} with C_L shown in figure 6 were cross-plotted from these data. In figure 7 these results have been summarized in the form of C_{l_p} at zero lift as a function of sweep. For the flapped wings a similar method was used to derive corresponding data shown in figure 8 in the form of the variation of C_{l_p} with C_L. In figure 9 is shown the variation of C_{l_p} with R for the various plain wings at zero lift. These curves were derived from plots similar to figure 6 for various values of dynamic pressure. Results of the pressure-distribution measurements in steady roll are shown in figures 10 and 11. True polar diagrams (reference 3) for each plain wing are presented in figure 12 for use in predicting probable regions of rolling instability. With the exception of figure 9, all the data presented in the foregoing figures were obtained at a dynamic pressure of 20 pounds per square foot.

The following discussion of the results of this investigation has been divided into three parts: (1) the effects of sweep on C_{l_p} at zero lift, (2) the effects of lift on C_{l_p}, and (3) the autorotational characteristics. In addition to the discussion of the experimental data, a brief analysis of theoretical methods of predicting the damping characteristics of swept wings is presented in parts (1) and (3). Some discussion of theory is given in part (2) in order to explain trends in the experimental results. Pressure-distribution data have been introduced in the analysis only for the purpose of interpreting portions of the measured damping-moment data.

Effects of Sweep at Zero Lift

Comparison of experiment with theory.- Results of this investigation, summarized in figure 7, clearly indicate the reduction in C_{l_p} at zero lift coefficient caused by sweeping the wing panels of a given plan form either forward or backward. This decrease results from the reduction in lift-curve slope attendant with sweep. Glauert first showed in reference 7 that the damping of a wing in roll is a function of $C_{L_\alpha} + C_D$. For the normal range of angle of attack the wing drag coefficient is negligible as compared with the lift-curve slope C_{L_α}, thereby leaving the damping dependent principally on C_{L_α}. From simple sweep theory and experiment it has been shown that C_{L_α} for swept wings varies approximately as $\cos \Lambda$ for constant aspect ratio. Thus, the damping in roll for swept wings would then be expected to vary similarly. Since in the present tests some variation in aspect ratio resulted from sweeping the fixed wing panels, a correction for aspect ratio variation was applied. This was done in order to show a comparison between the swept-wing test data and the damping characteristics of the swept wings as projected by simple sweep theory from the measured value of C_{l_p} for the unswept wing. These corrections for sweep and aspect ratio were applied in the following manner:

$$\left(C_{l_p}\right)_\Lambda = \left(C_{l_p}\right)_{\Lambda=0} \times \cos\Lambda \times \frac{\left(\frac{A}{A+4}\right)_\Lambda}{\left(\frac{A}{A+4}\right)_{\Lambda=0}}$$

where the subscript Λ refers to the swept wings and the subscript $\Lambda = 0$ refers to the wing tested with zero sweep. The term $\frac{A}{A+4}$ is a rolling-moment induction factor (reference 2) derived from lifting-line theory with the aspect ratio A based on the over-all geometric span. The projected values of damping at sweep given in figure 7 conform well with the measured values of C_{l_p}, with a maximum deviation of 4 percent for the 45° swept-forward wing.

Two further comparisons, both of which involve a variation of the aspect-ratio correction, are shown in figure 7 in the form of additional projections of the damping at sweep based on the unswept-wing data. For the first comparison a modified rolling-moment induction factor $\frac{A}{AE'_{e_c} + 4}$ was employed, where E'_{e_c} is an effective edge-velocity correction based on lifting-surface theory. (See reference 5.) Because of the moderate variation in aspect ratio of the test wings, the effect of this edge correction was small for all the wings except the highly swept-forward wing, where the aforementioned deviation of 4 percent increased to 11 percent. For the other comparison a term $\frac{A'}{A' + 4}$ was used as the aspect-ratio correction, where A' is the aspect ratio based on the length of the quarter-chord line rather than on the true geometric span. As can be noted in figure 7 this procedure resulted in poor agreement with the experimental values of C_{l_p} and does not support the theory posed in earlier swept-wing work to the effect that the quarter-chord line rather than the true span possibly should be used for determining the effective aspect ratio of a swept wing.

Predicted damping characteristics.— Since rolling tests of a new wing design are rarely possible, estimated rotary-damping characteristics have to be relied upon for dynamic-stability calculations. While fairly accurate methods of predicting the value of C_{l_p} for conventional unswept wings are available, no such analyses for swept wings exist at the present time in published form. Two different methods appear to offer the most suitable means of predicting the damping in roll for swept wings which are as follows: (1) estimate C_{l_p} for an equivalent unswept wing and correct this value by sweep theory, and (2) compute the damping directly for the swept wing by employing a theoretical method of determining span loading, such as proposed by Weissinger. (See reference 4.)

A comparison of the two methods is made in figure 7. For the first procedure, three different values of C_{l_p} for the test unswept wing are shown. Two of these values were determined from curves in references 5 and 6, while the third value was computed by the Weissinger method. The closest agreement with the experimental measurement of C_{l_p} (1-percent deviation) was given by the estimate from lifting-surface theory. This value was obtained by a slight extrapolation of data from reference 5, which were increased by 6 percent as recommended in references 8 and 9 to correct for the effect of square tips. In the case of the value of C_{l_p} computed for the unswept wing by Weissinger's method, which was 7 percent low, it was found that consideration of either 7 or 15 spanwise stations in the theoretical computations made no perceptible difference in the final answer. Since, as noted previously, the application of sweep theory enabled prediction of the effects of sweep within 4 percent, it follows that the damping in roll for a swept wing can be predicted within 5 percent by applying sweep theory to a lifting-surface-theory estimate of C_{l_p} for the unswept wing.

In the second case, where the damping of a swept wing was computed directly by use of Weissinger's method, the results disagreed with experiment to such an extent that the method appears unreliable. The deviation of the computed C_{l_p} from the measured value varied from 11 percent high for the 45° swept-back wing to 7 percent low for the 0° swept wing, while the computed results for the other three wings showed good agreement with the experimental data. Here again consideration of 15 spanwise stations in the computations as compared with 7 stations showed no significant difference in the results for any of the wings.

From an over-all analysis of the results shown in figure 7, it may be concluded that the optimum method, from the standpoint of both reliability and least amount of computation, of predicting the damping in roll for a given swept-forward or swept-back wing is as follows: (1) estimate the C_{l_p} for an unswept wing with the same aspect ratio, taper ratio, and section characteristics as the swept wing using curves computed from lifting-surface theory (reference 5), and (2) correct this value of C_{l_p} for the effect of the reduction in lift-curve slope due to sweep.

Reynolds number effect.– The influence of a variation in Reynolds number on C_{l_p} for each of the swept wings at zero lift is shown in figure 9. Sweep apparently has little if any effect on the variation in damping with Reynolds number, since the variation was uniform for all the wings except the 45° swept-forward wing. Tests at Reynolds numbers ranging from 5,600,000 to 20,400,000 (based on the M.A.C.) showed for C_{l_p} values of each wing an increase which varied from 8 percent for the unswept wing to 28 percent for the 45° swept-forward wing. Approximately 5 percent of this increase is attributable to first-order compressibility effects. Such a large increment in C_{l_p} due to Reynolds number as was measured for the highly swept-forward wing cannot be readily explained. A possibility exists that, owing to the rather large damping-in-roll torque (up to 50,000 lb-ft), there was some twisting of the wing panels. However, if deflection accounts for some of the increase, then the damping of the 45° swept-back wing should have decreased, since the same panels were employed in both plan forms.

It should be noted that the experimental results used for the comparison in figure 7 were measured at a constant test dynamic pressure and therefore represent data obtained at various Reynolds numbers based on the M.A.C. At the present time there is doubt as to what dimension should be used in computing the Reynolds number for swept wings. From the concepts of simple sweep theory it appears that a dimension perpendicular to the quarter-chord line should be used to define R, in which case the test results of figure 7 would represent data at an approximately constant R. However, even if values of C_{l_p} at a constant Reynolds number based on the M.A.C. are used in the comparison of figure 7, the main conclusions still apply. Such a comparison at a Reynolds number of 10,000,000 indicates that predicted values of C_{l_p} for the swept wings calculated by the method previously recommended are within 6 percent of the measured values of damping shown in figure 9 for this constant R.

Effects of Lift

Plain wings.- The variations of C_{l_p} with angle of attack and lift coefficient are shown in figures 5 and 6, respectively, for each of the five wings. The damping increased moderately in the usual lift range below the stall for all the wings except the 45° swept-forward wing. For this wing a 104-percent increase in damping was observed between the C_L limits of 0 and 1.05. An accurate check of these characteristics was obtained from a spanwise integration of the antisymmetric wing loadings as determined from pressure-distribution measurements. These data for each wing at three angles of attack are presented first in figure 10 as the spanwise wing-loading increment generated in steady roll, and in figure 11 as section lift-coefficient characteristics.

Some increase in damping (approximately 2 percent for the unswept wing over the linear portion of the lift curve) can be attributed to the rotation of the resultant force vector at each section due to the change in angle of attack along the wing. In the case of the 45° swept-forward plan form the combined effect of the nonlinear lift-curve slope (note in fig. 5(a)) and the rocking of the resultant force vector accounts for approximately 30 percent of the increase in damping. The remainder is attributed to the fact that, as may be noted in figure 11(a), the wing-section lift-curve slopes are not constant with angle of attack, but rise sharply (approximately 100-percent increase) at the outboard wing sections, probably owing principally to the drainage of the boundary layer away from the tips toward the center section.

Flapped wings.— A limited amount of damping-in-roll data was obtained for each wing with partial-span split flaps deflected 60°. The results given in figure 8 were determined principally to define the region of autorotation and are therefore inadequate to show clearly the variation in damping over the complete range of angle of attack. However, the results do indicate that the value of C_{l_p} near maximum lift with flaps deflected is approximately the same as the maximum value of damping measured for the plain wing.

Autorotational Characteristics

Tests at angles of attack above the normal operating range were included in the present investigation for the purpose of determining the tendencies toward autorotation and regions of autorotation for each of the five wings, both plain and flapped. The results, shown in figures 3 and 4 for the plain and flapped wings, respectively, have been presented only in the form of the rolling-moment coefficient C_l as a function of the wing-tip helix angle $pb/2V$. No attempt has been made to evaluate C_{l_p} in the unstable region in view of the fact that, when a wing approaches an unstable condition, C_l ceases to be a linear function of $pb/2V$ and the value of C_{l_p} then has little significance.

A general comparison of the results indicates that sweep reduces and flaps increase the magnitude of the autorotational moment. For either the highly swept-forward or highly swept-back plain wing the maximum angle of attack attainable with the apparatus (29°) was not sufficient to permit autorotation. However, installation of 60° split flaps on these two highly swept wings caused instability for the 45° swept-back wing but caused the 45° swept-forward wing to become a little more stable.

From the data it can be observed that for the unswept and swept-forward wings autorotation occurred at an angle of attack beyond the stall peak. This phenomenon is explainable by Glauert's general theory for the autorotation of a wing (reference 7), in which the region of rotary instability is determined by the criterion

$$C_{L_\alpha} + C_D < 0$$

where the angle of attack α is in radians. This theory is based on the supposition that the section characteristics are constant across the span. Since C_D is always positive, autorotation will occur when the negative slope of C_{L_α} beyond the stalling angle is sufficiently great to outweigh the value of C_D. Therefore, from a true polar diagram for the wing the probable limits of angle of attack for autorotation can be determined graphically. Any point on the polar curve at which the slope is perpendicular to a radial line through the origin of the coordinate axes would, from Glauert's criterion, indicate an attitude of the wing where either autorotation sets in or stability returns.

In figure 12, true polar diagrams for each plain wing (reference 3) are presented together with the angle of attack for rotary instability as predicted and as measured experimentally. In this comparison it will be noted that the theoretical predictions agreed well with the test data, as far as it went, for the unswept and swept-forward plan forms, while little conformity resulted with the swept-back plan forms. This is understandable because, as noted previously, the theory is based on the assumption that the section characteristics are constant along the span; this assumption is especially important for the outboard sections, which exert the greatest influence on the damping characteristics. Such a condition of uniformity is not realized across the span for the swept-back plan forms, since the efficiency of the outer sections of the swept-back wing is impaired by the spanwise drainage of the boundary layer toward the tips. In figures 3(d) and 12 the data show that the 30° swept-back wing autorotated at an angle of attack of 19°, which is below the stall peak. This result is confirmed by the span-loading-increment variation determined from the measured pressure data which is shown in figure 10(b) for this attitude.

From these results it may be concluded that Glauert's autorotation theory provides a fairly reliable indication of the autorotational characteristics for unswept and swept-forward wings of the type investigated but is unreliable for wings, such as those with sweepback, which possess early tip-stalling characteristics.

CONCLUSIONS

From wind-tunnel tests to determine the damping-in-roll characteristics of large-scale tapered wings having angles of sweep of 0°, ±30°, and ±45° the following conclusions may be drawn:

1. The damping-in-roll parameter C_{l_p} for swept wings at zero lift decreased proportionally to the cosine of the angle of sweep for constant aspect ratio based on the conventional span.

2. The value of C_{l_p} for swept-forward or swept-back wings at zero lift can be predicted within 6 percent by estimating the C_{l_p} for an equivalent unswept wing by lifting-surface theory and correcting this value for the effects of sweep by simple sweep theory.

3. Results of Weissinger's theoretical span-loading computations for the C_{l_p} of each wing were inconsistent with the experimental data.

4. For an increase in Reynolds number of approximately 10,000,000 the C_{l_p} at zero lift increased gradually and uniformly for all sweep angles except in the case of the 45° swept-forward wing, where a relatively large increase of 28 percent occurred.

5. Below the stall, C_{l_p} increased moderately with lift coefficient for each of the wings except in the case of 45° swept-forward wing which exhibited a 104-percent increase. Pressure-distribution measurements showed that over an outboard portion of this wing the section lift-curve slope almost doubled throughout the lift range, and this change accounted for a major portion of the abnormal variation in damping.

6. Deflection of partial-span split flaps had no appreciable effect on the value of C_{l_p} for the wings near maximum lift.

7. The magnitude of the autorotational moment was reduced by sweep and augmented by the deflection of partial-span split flaps.

8. Glauert's theory for autorotation is fairly reliable for predicting regions of rotary instability for unswept and swept-forward wings of the type investigated but is not applicable to

wings, such as those with sweepback, which possess early tip-stalling characteristics.

Ames Aeronautical Laboratory,
National Advisory Committee for Aeronautics,
Moffett Field, Calif.

Lynn W. Hunton

Lynn W. Hunton,
Aeronautical Engineer.

Joseph K. Dew

Joseph K. Dew,
Aeronautical Engineer.

Henry J. Goett

Approved:

for John F. Parsons,
Aeronautical Engineer.

REFERENCES

1. Glauert, H.: The Elements of Airfoil and Airscrew Theory. Cambridge University Press, 1926.
2. Munk, Max M.: Fundamentals of Fluid Dynamics for Aircraft Designers. The Ronald Press Co., 1929.
3. McCormack, Gerald M., and Stevens, Victor I.: An Investigation of the Low-Speed Stability and Control Characteristics of Full-Scale Swept-Forward and Swept-Back Wings. NACA RRM No. A6K15, 1946.
4. Van Dorn, Nicholas H., and DeYoung, John: A Comparison of Three Theoretical Methods of Calculating Load Distribution on Swept Wings. NACA RRM No. A7C31, 1947.
5. Swanson, Robert S., and Priddy, E. LaVerne: Lifting-Surface-Theory Values of the Damping in Roll and of the Parameter Used in Estimating Aileron Stick Forces. NACA ARR No. L5F23, 1945.
6. Pearson, H.A.: Theoretical Span Loading and Moments of Tapered Wings Produced by Aileron Deflection. NACA TN No. 589, 1937.
7. Glauert, H.: The Investigation of the Spin of an Aeroplane. R & M No. 618, British A.R.C., 1919.
8. Swanson, Robert S., and Toll, Thomas A.: Estimation of Stick Forces from Wind-Tunnel Aileron Data. NACA ARR No. 3J29, 1943.
9. Pearson, Henry A., and Jones, Robert T.: Theoretical Stability and Control Characteristics of Wings With Various Amounts of Taper and Twist. NACA Rep. No. 635, 1938.

TABLE I

INDEX TO THE BASIC-DATA FIGURES

Wing condition	q (lb/sq ft)	α_u (deg)	Figure number: C_l vs $pb/2V$	Figure number: $\Delta\left(\frac{c_l c}{pb/2V}\right)$ vs span	Figure number: C_{l_p} vs R
−45° plain	20	−1, 1.5, 4, 9, 14, 19, 24, 29	3(a)	10(a)	9
plain	60	−1			9
plain	120	−1			9
flapped	20	14, 19, 24, 29	4(a)		
−30° plain	20	−1, 1.5, 4, 9, 14, 19, 24, 29	3(b)	10(a)	9
plain	60	−1			9
plain	120	−1			9
flapped	20	14, 19, 24, 29	4(a)		
0° plain	20	−1, 1.5, 4, 9, 14 19, 24	3(c)	10(b)	9
plain	60	−1			9
plain	120	−1			9
flapped	20	14, 19, 24	4(b)		
30° plain	20	−1, 1.5, 4, 9, 14 19, 24, 29	3(d)	10(b)	9
plain	60	−1			9
plain	120	−1			9
flapped	20	9, 14, 19, 24	4(c)		
45° plain	20	−1, 1.5, 4, 9, 14 19, 24, 29	3(e)	10(b)	9
plain	60	−1			9
plain	125	−1			9
flapped	20	9, 14, 19	4(c)		

TABLE II

DAMPING-IN-ROLL CORRECTION DUE TO SIDESLIP

α_u (deg)	Wing condition	ΔC_{l_p}				
		$-45^{\circ}\Lambda$	$-30^{\circ}\Lambda$	$0^{\circ}\Lambda$	$30^{\circ}\Lambda$	$45^{\circ}\Lambda$
0	plain	0	0	0	0	0
9	plain	-.005	-.004	0	0	-.002
	flapped	-.012	-.009	0	0	-.003
14	plain	-.012	-.008	.002	0	-.004
	flapped	-.022	-.014	0	0	-.006
19	plain	-.021	-.009	.003	0	-.005
	flapped	-.029	-.019	0	0	0
24	plain	-.026	-.005	0	0	-.004
	flapped	-.032	0	0	0	0
29	plain	-.023	0	0	0	0
	flapped	0	0	0	0	0

1947

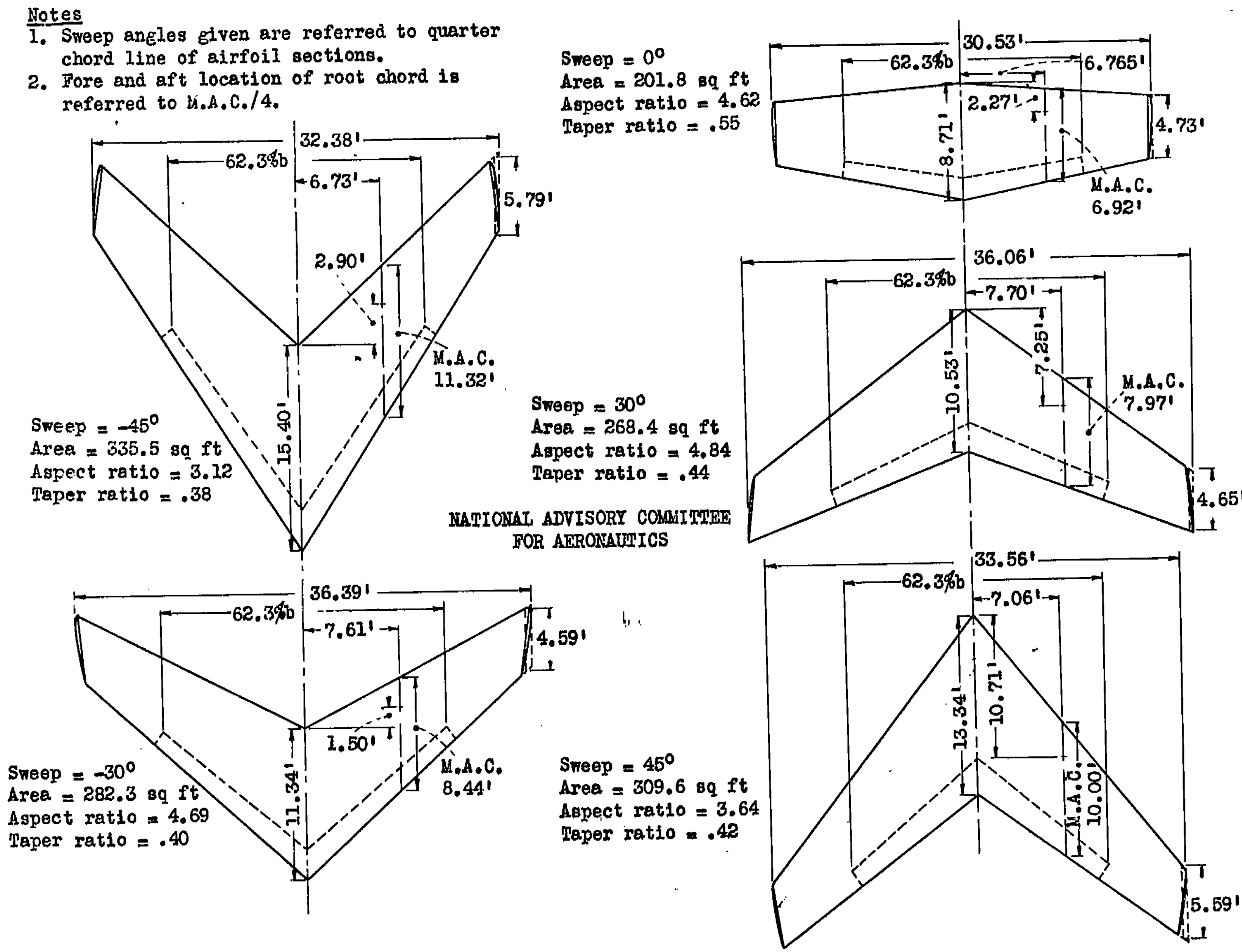

Figure 1.- Geometric characteristics of the swept wings.

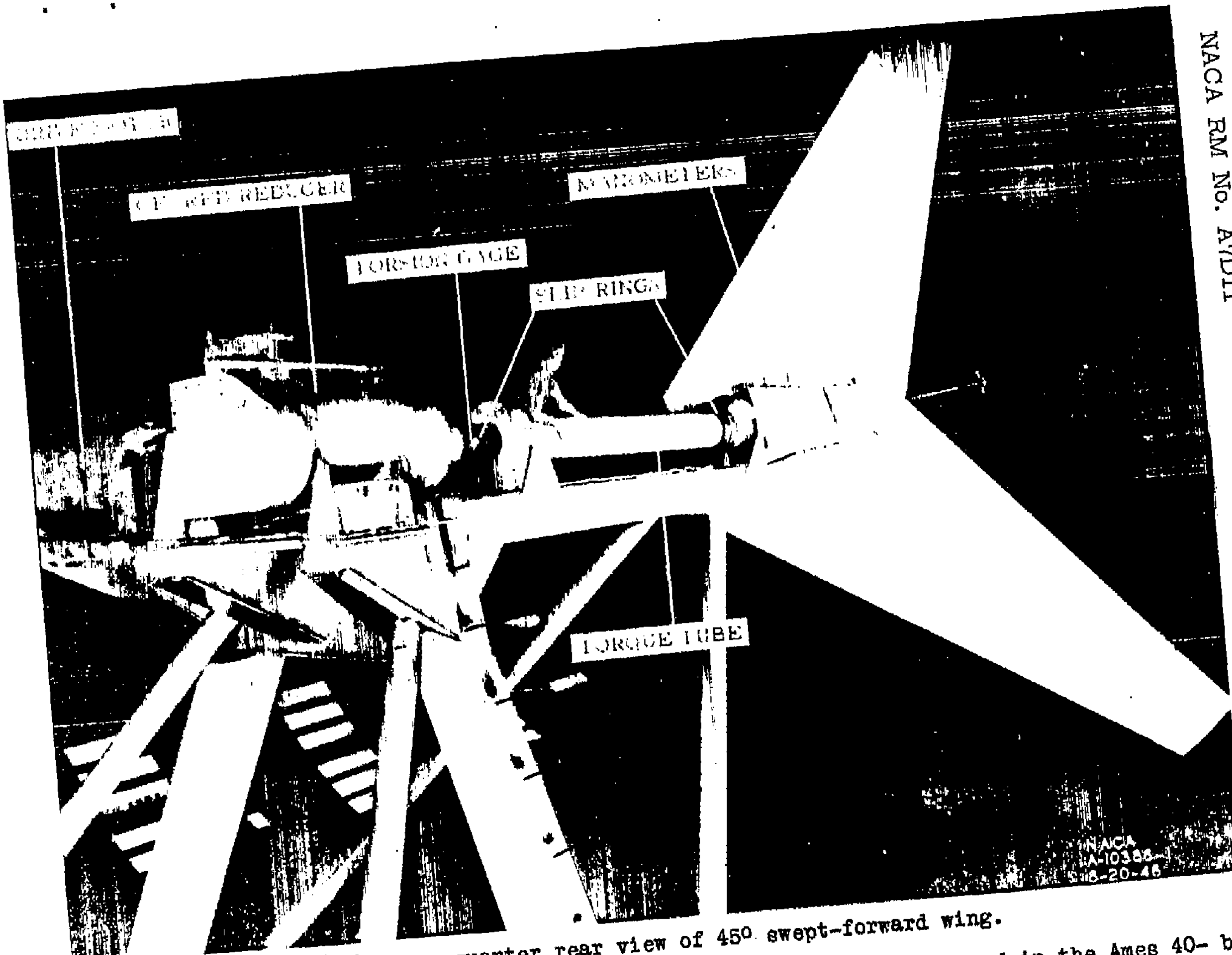

(a) Three-quarter rear view of 45° swept-forward wing.

Figure 2a to c.- Views of the swept wings mounted on the rolling wing stand in the Ames 40- by 80-foot wind tunnel.

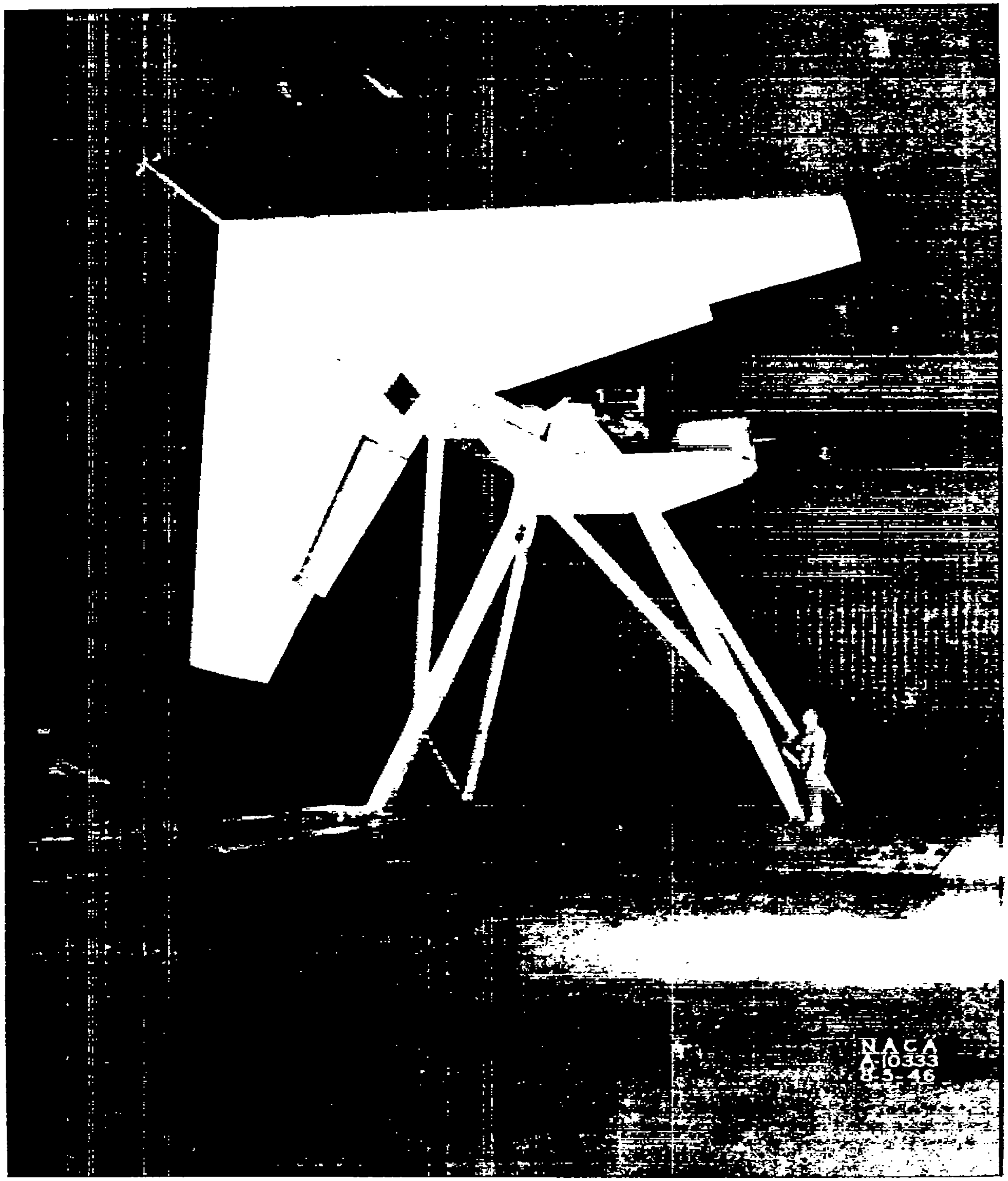

(b) Front view of 45° swept-back wing with split flaps deflected 60°.

Figure 2.- Continued.

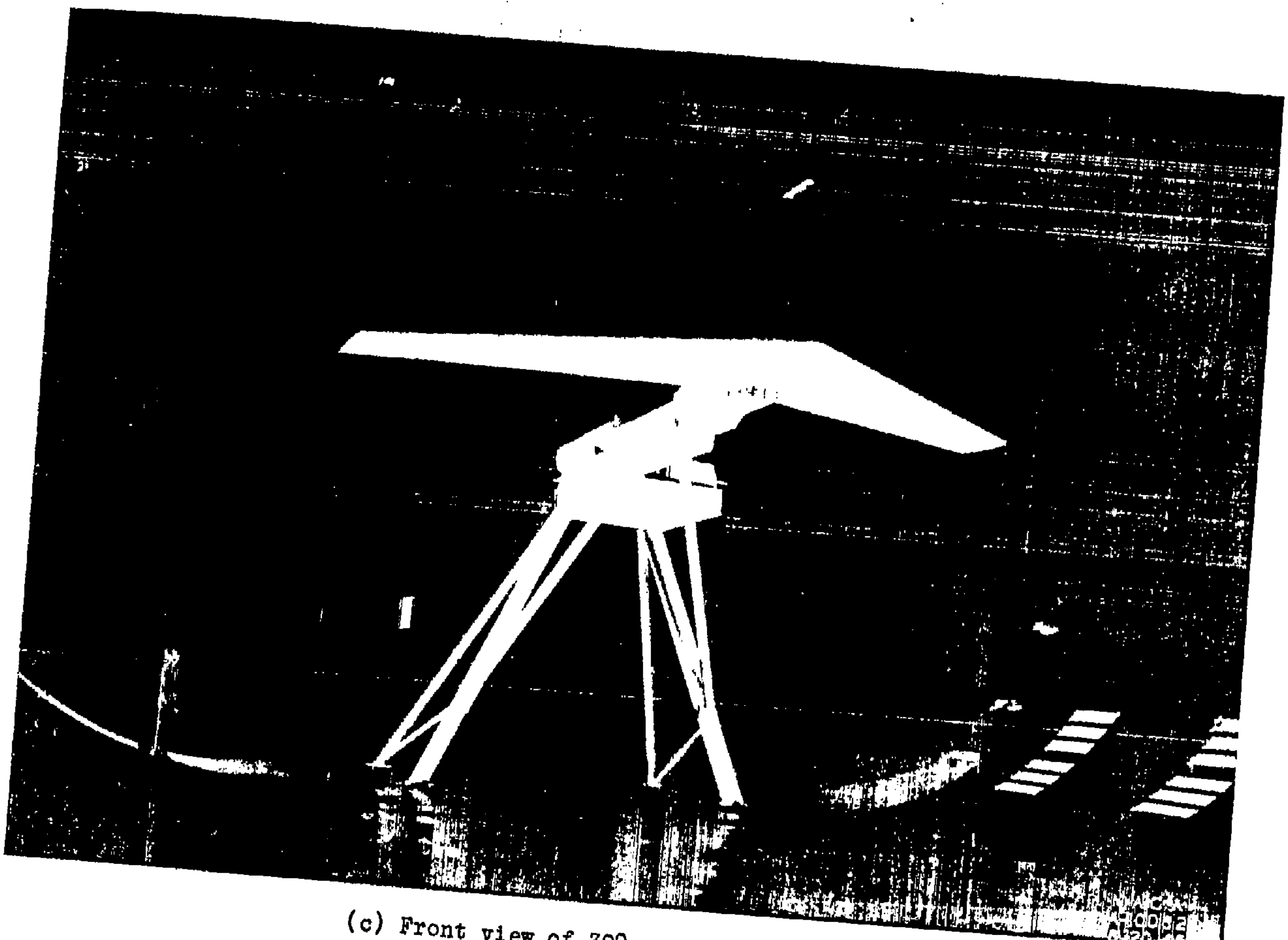

(c) Front view of 30° swept-back wing.

Figure 2.- Concluded.

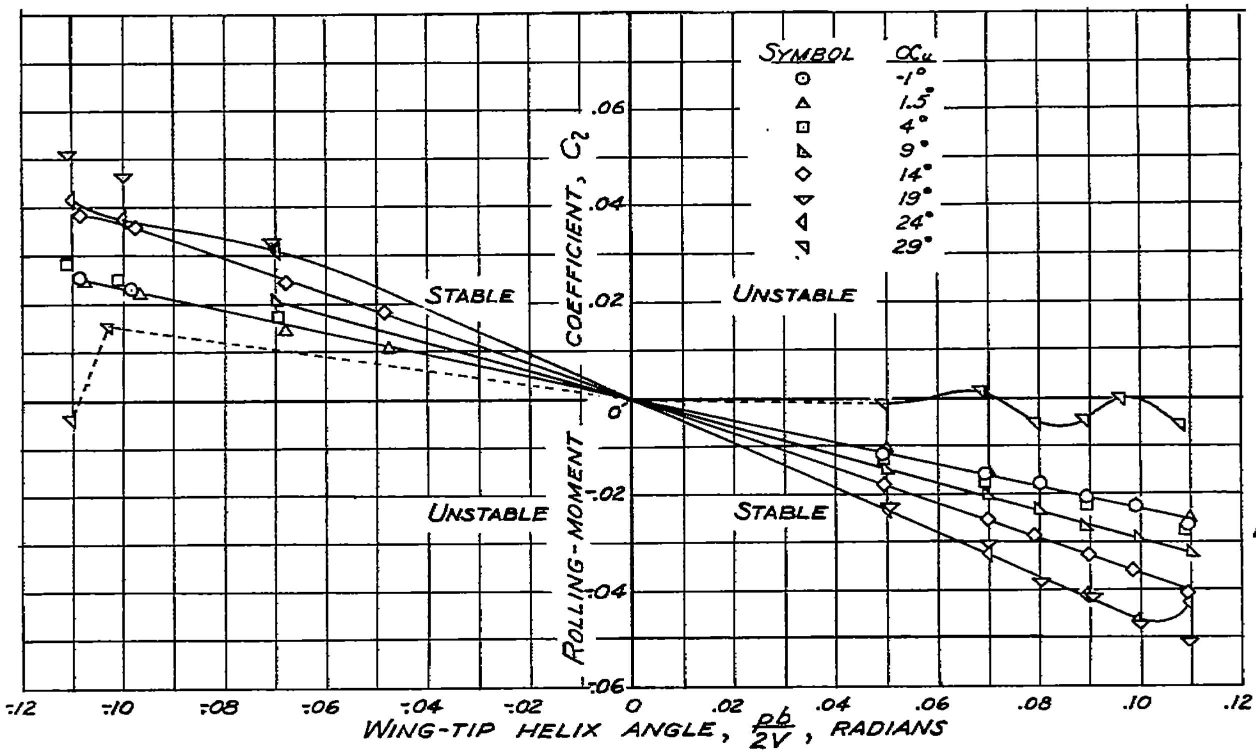

(a) 45° SWEPT-FORWARD WING.

FIGURE 3.— VARIATION OF ROLLING-MOMENT COEFFICIENT WITH WING-TIP HELIX ANGLE. PLAIN WINGS.

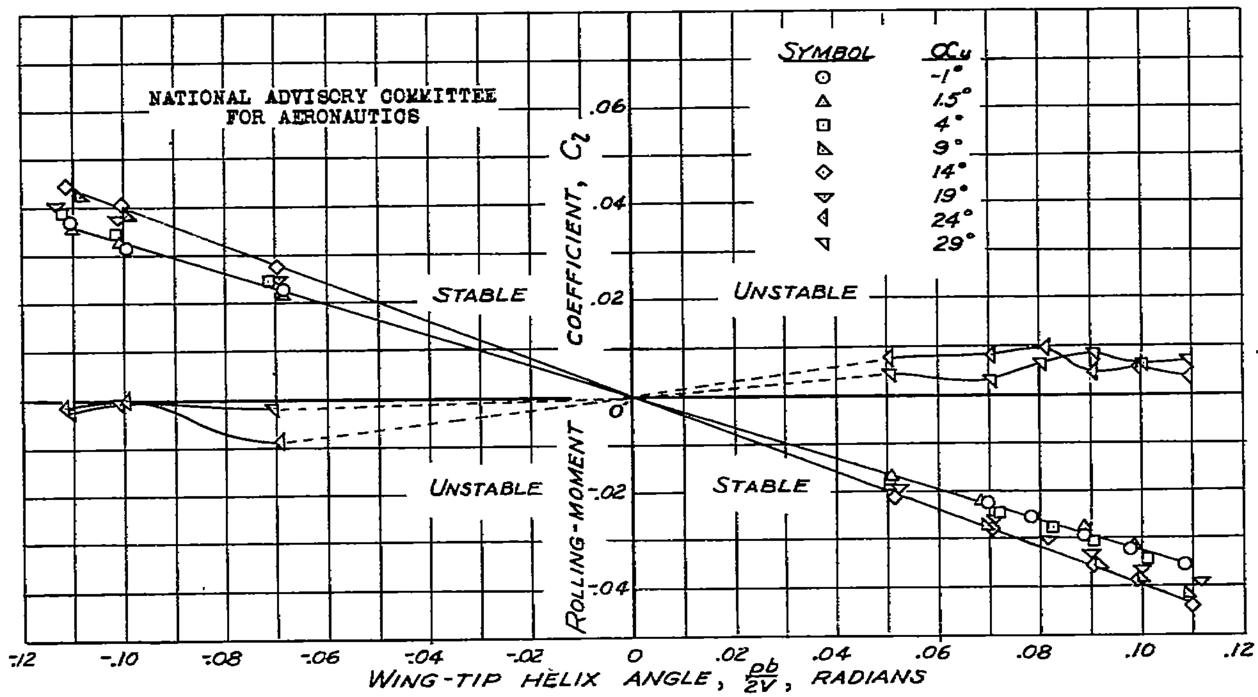

(b) 30° SWEPT-FORWARD WING.

FIGURE 3.- CONTINUED.

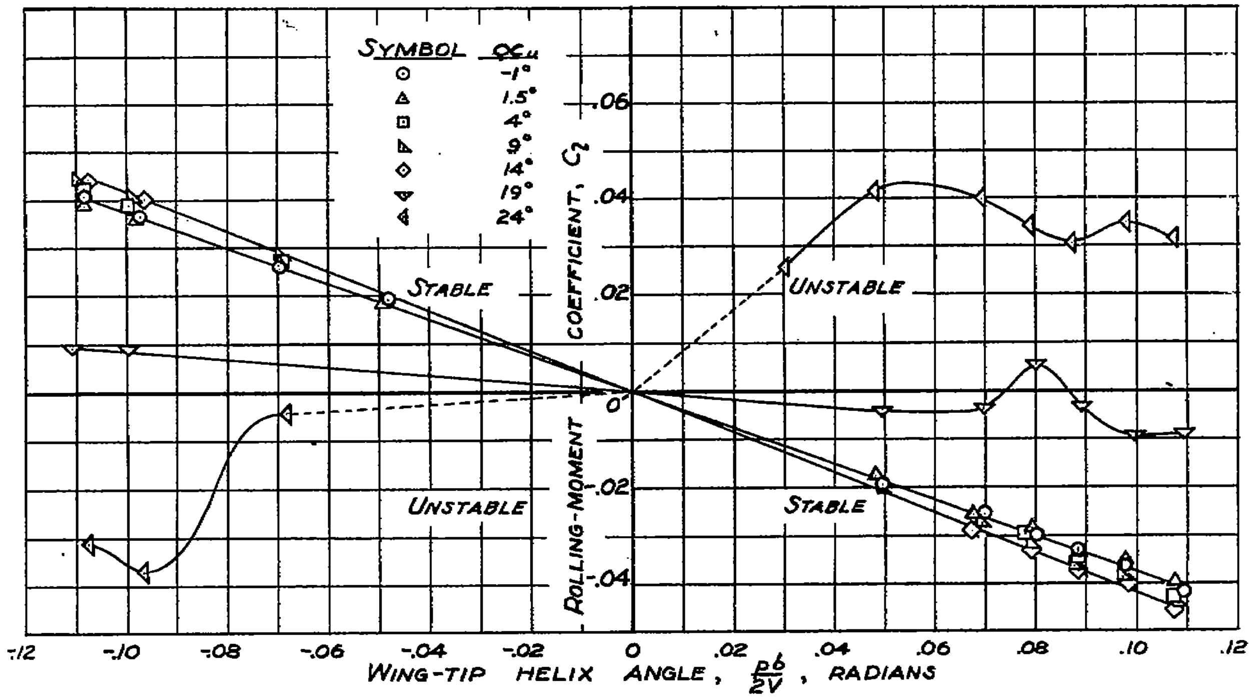

(c) 0° SWEPT WING.

FIGURE 3.– CONTINUED.

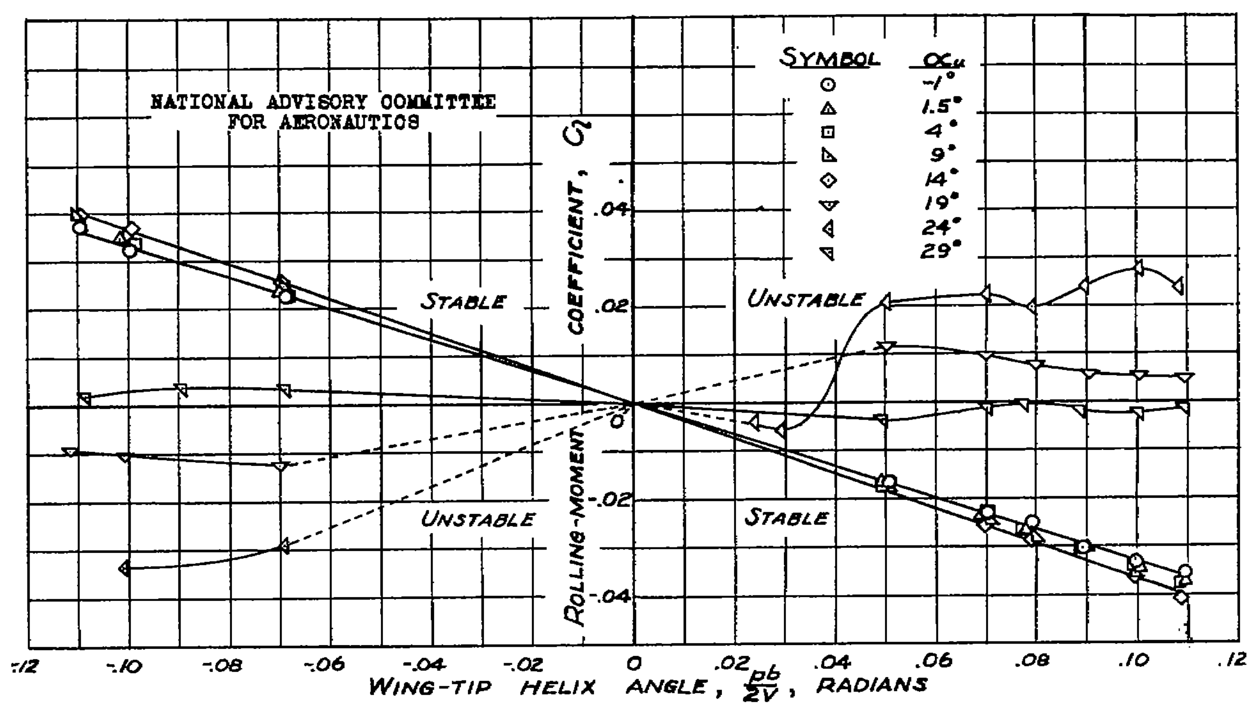

(d) 30° SWEPT-BACK WING.

FIGURE 3.– CONTINUED.

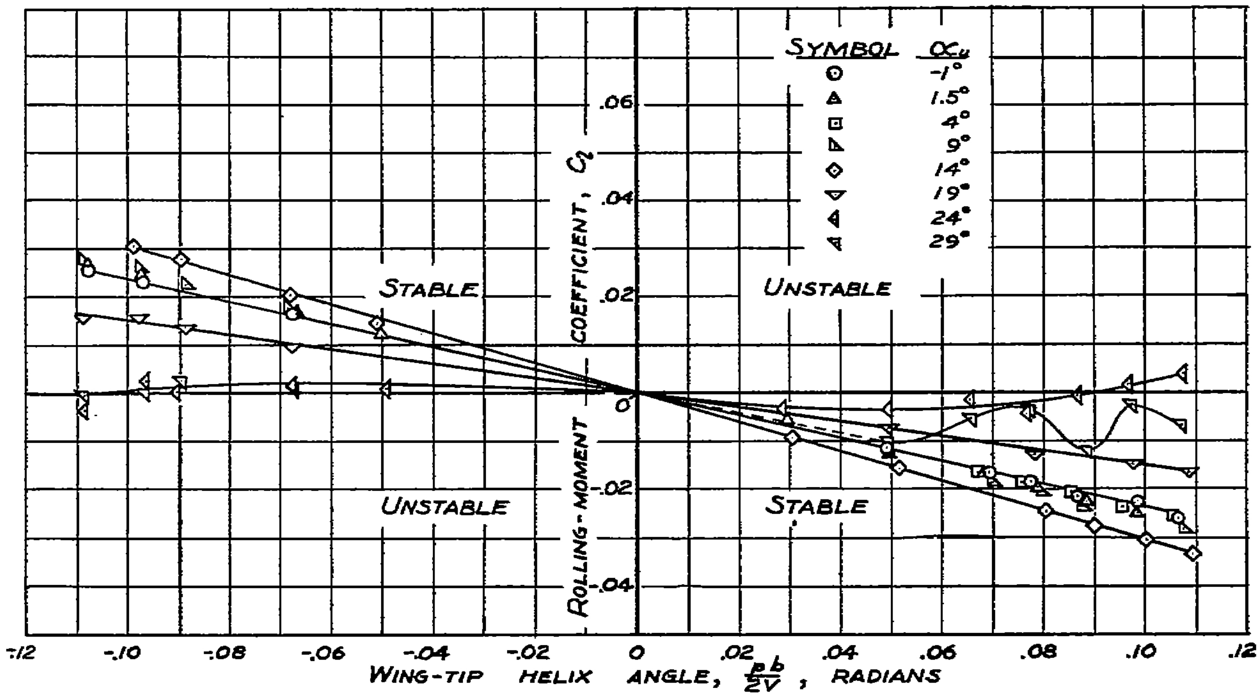

(e) 45° SWEPT-BACK WING.

FIGURE 3.– CONCLUDED.

NATIONAL ADVISORY COMMITTEE
FOR AERONAUTICS

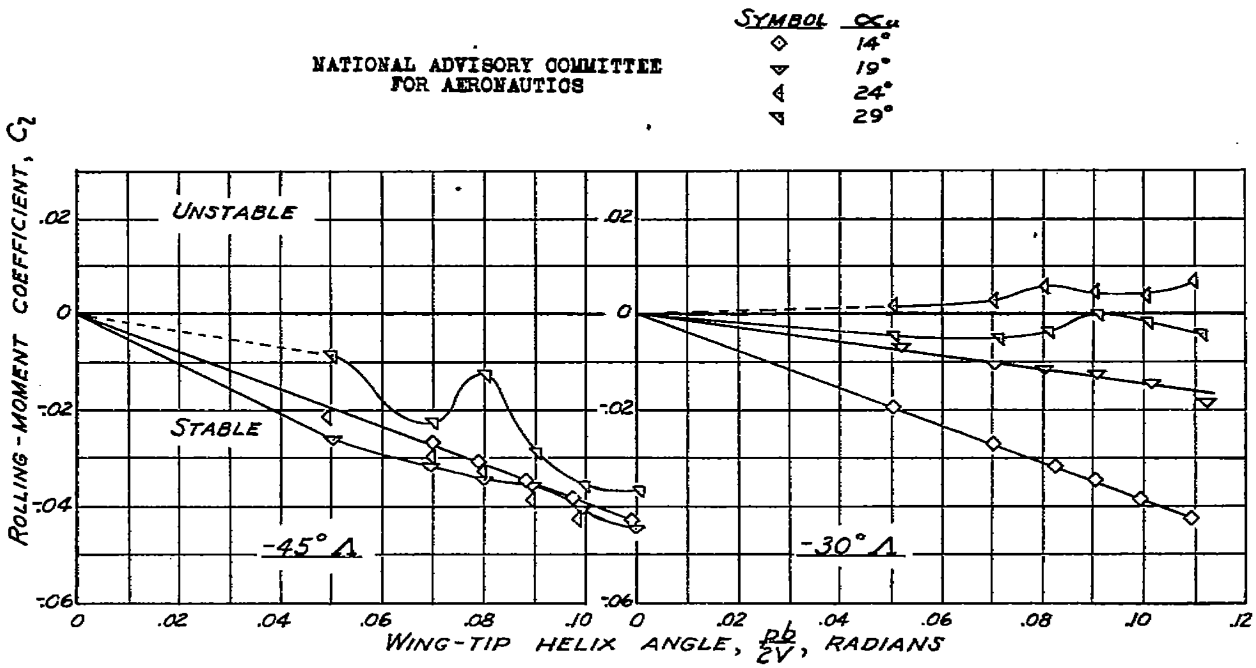

(a) 45° AND 30° SWEPT-FORWARD WINGS.

FIGURE 4.– VARIATION OF ROLLING-MOMENT COEFFICIENT WITH WING-TIP HELIX ANGLE. FLAPPED WINGS.

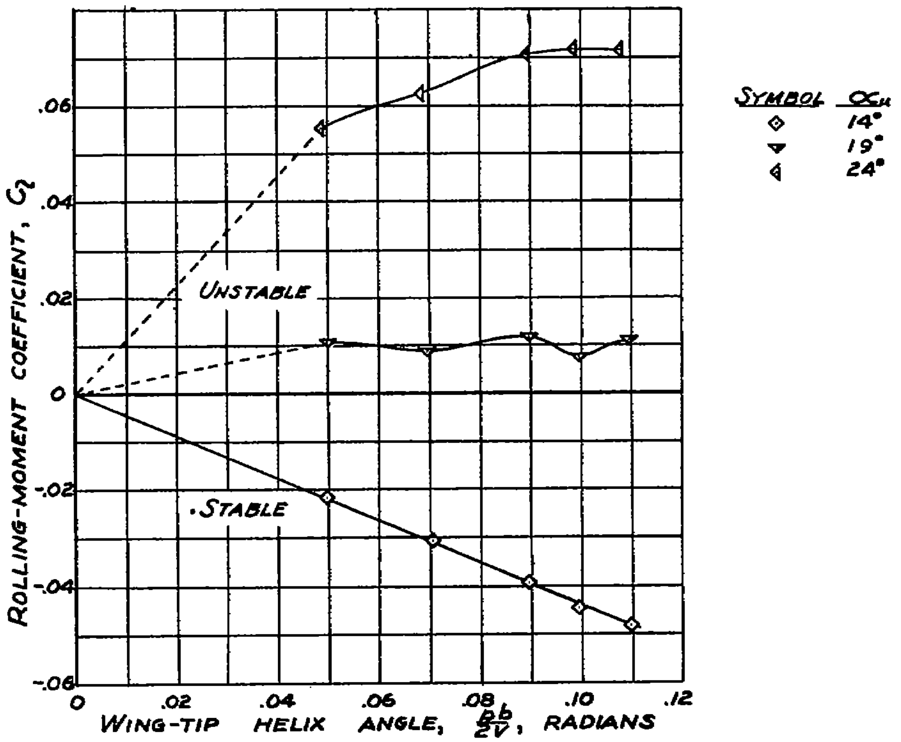

(b) 0° SWEPT WING.

FIGURE 4.— CONTINUED.

NATIONAL ADVISORY COMMITTEE FOR AERONAUTICS

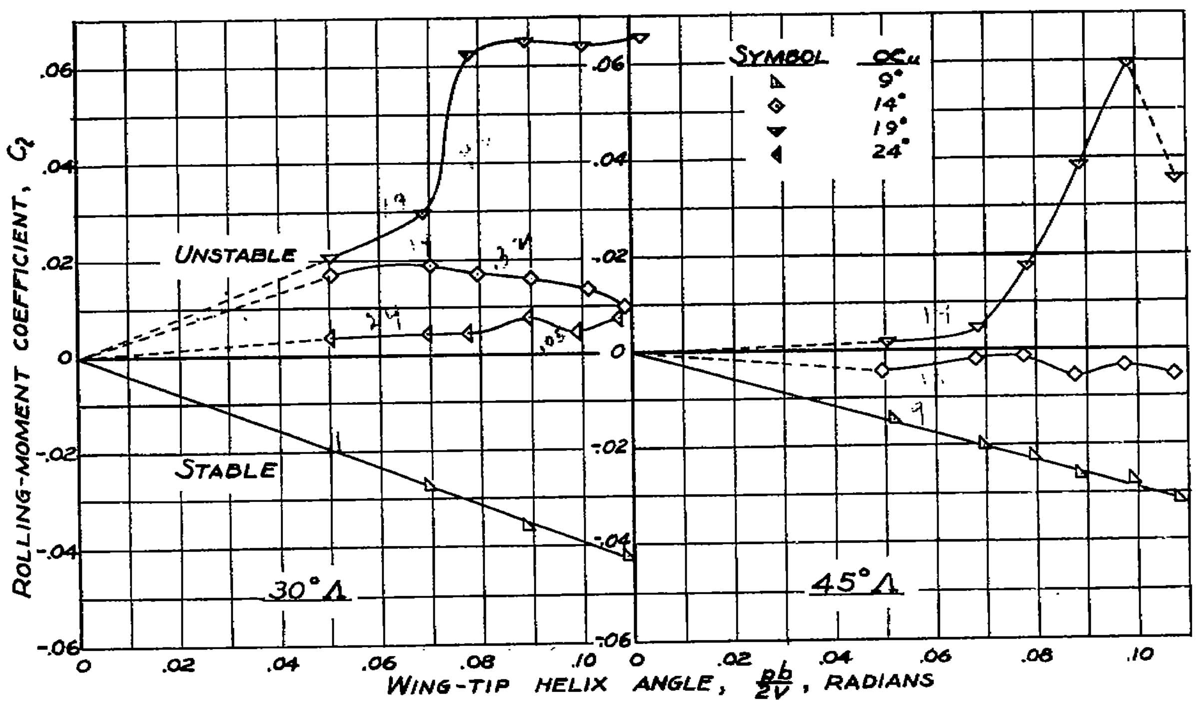

(c) 30° AND 45° SWEPT-BACK WINGS.

FIGURE 4.— CONCLUDED.

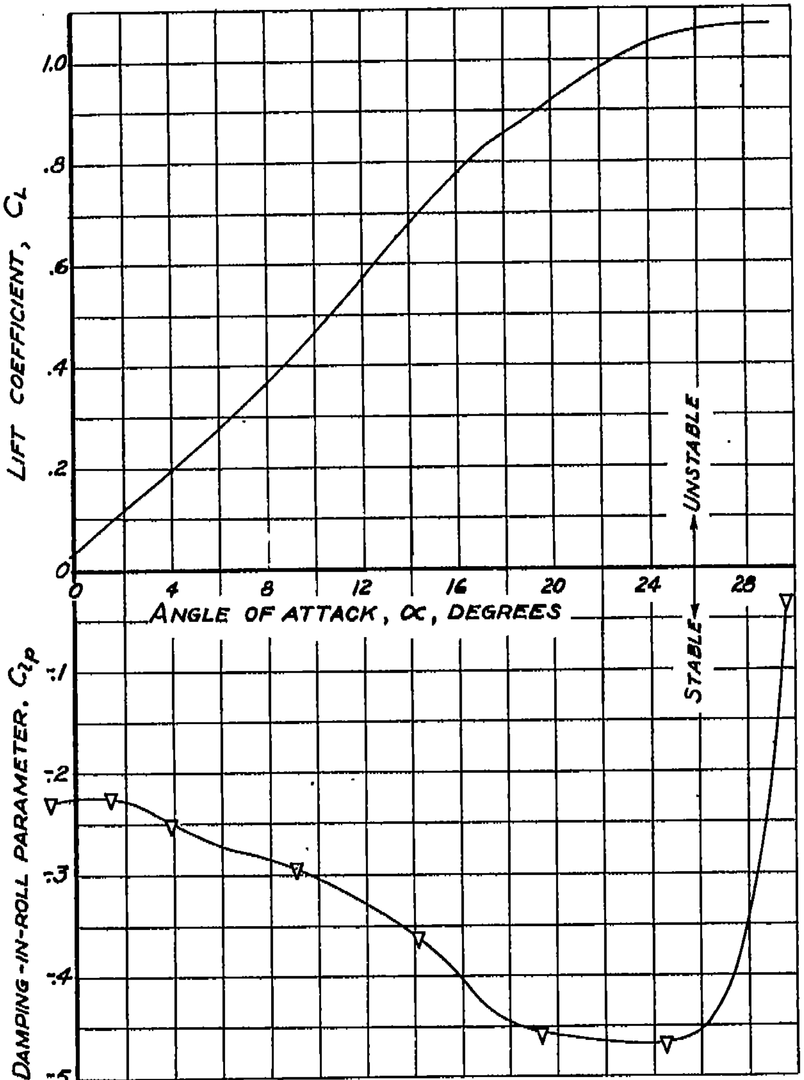

(a) 45° SWEPT-FORWARD WING.

FIGURE 5.– VARIATION WITH ANGLE OF ATTACK OF DAMPING-IN-ROLL PARAMETER AND LIFT COEFFICIENT. PLAIN WINGS.

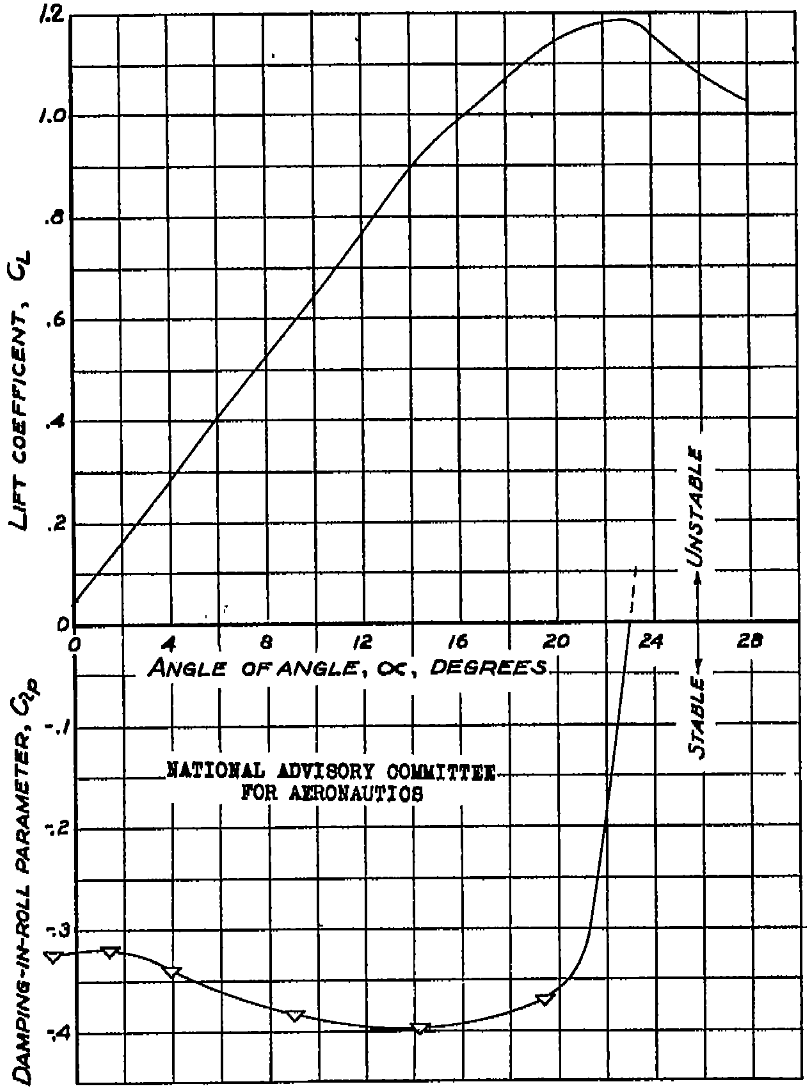

(b) 30° SWEPT-FORWARD WING.

FIGURE 5.– CONTINUED.

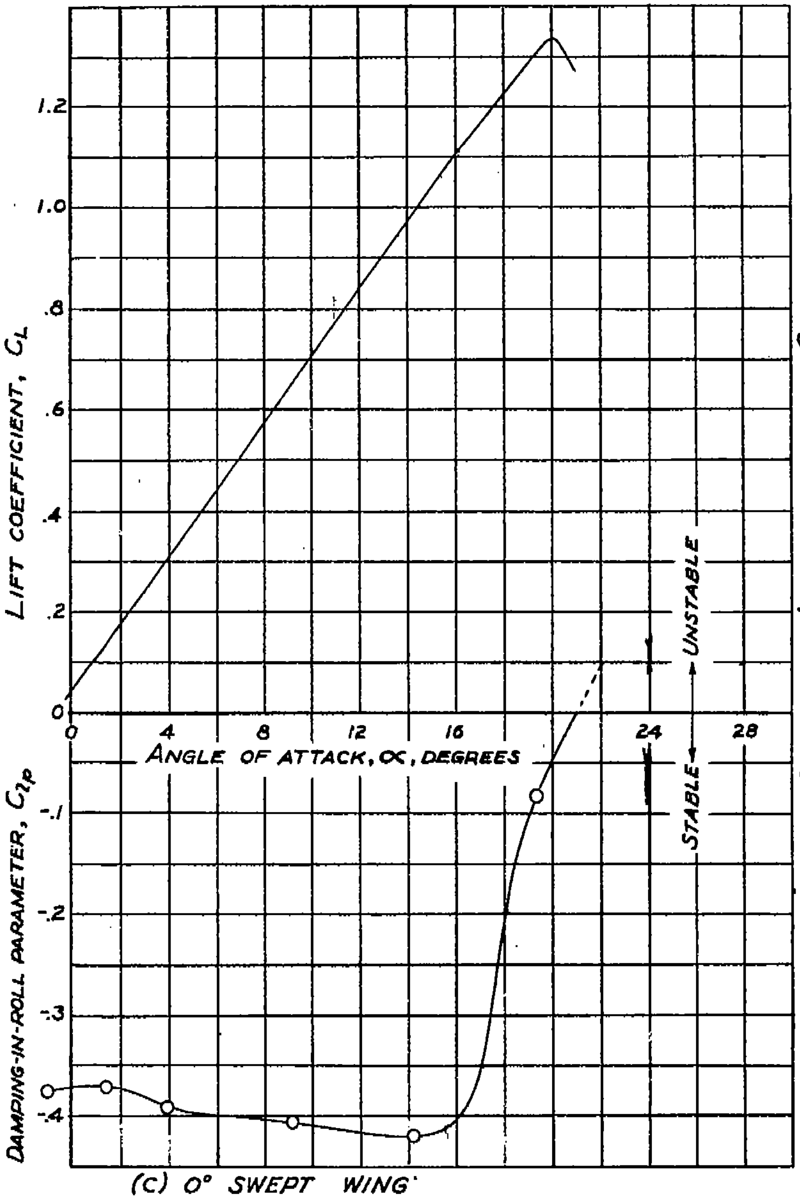

FIGURE 5.- CONTINUED.

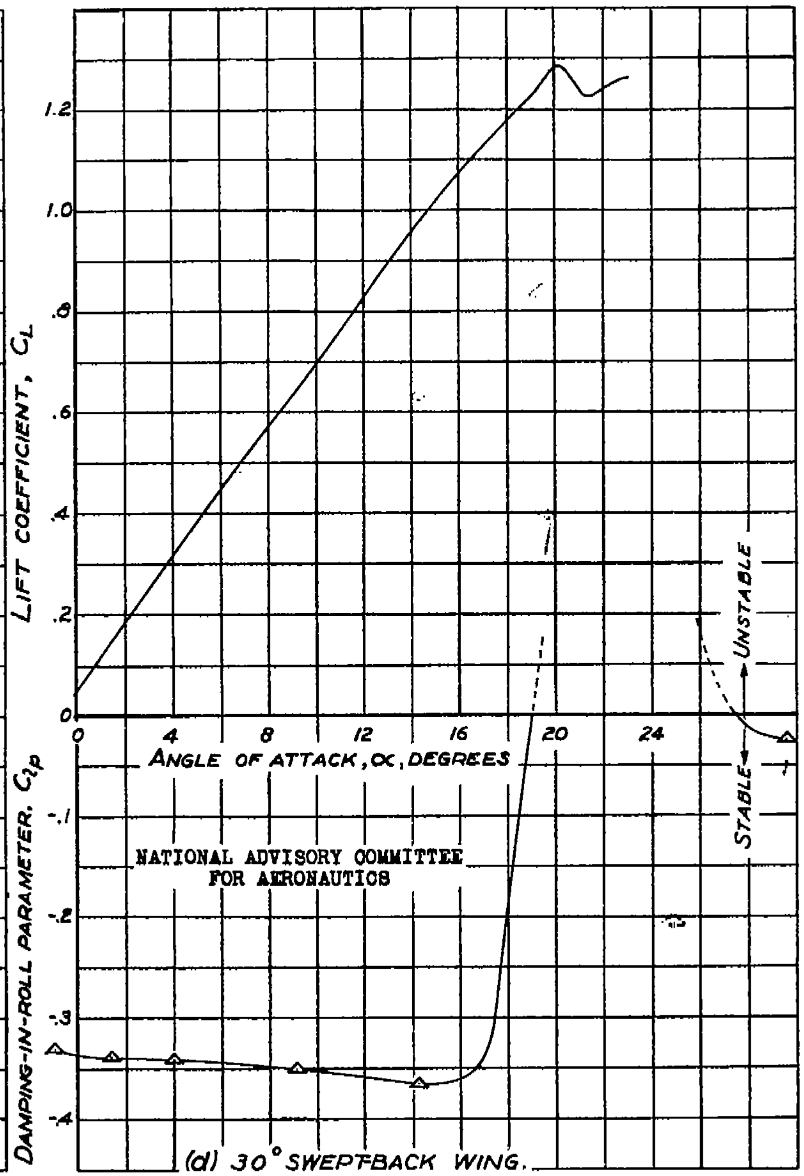

FIGURE 5.- CONTINUED.

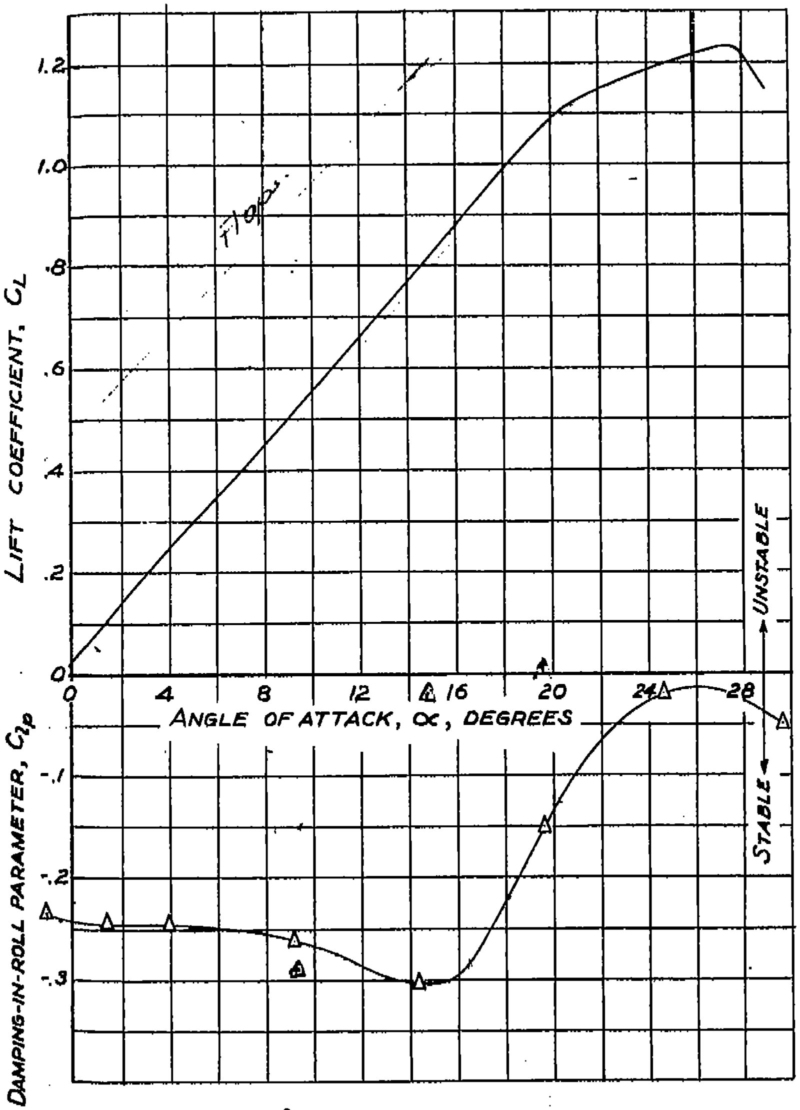

(e) 45° SWEPT-BACK WING.

FIGURE 5. – CONCLUDED.

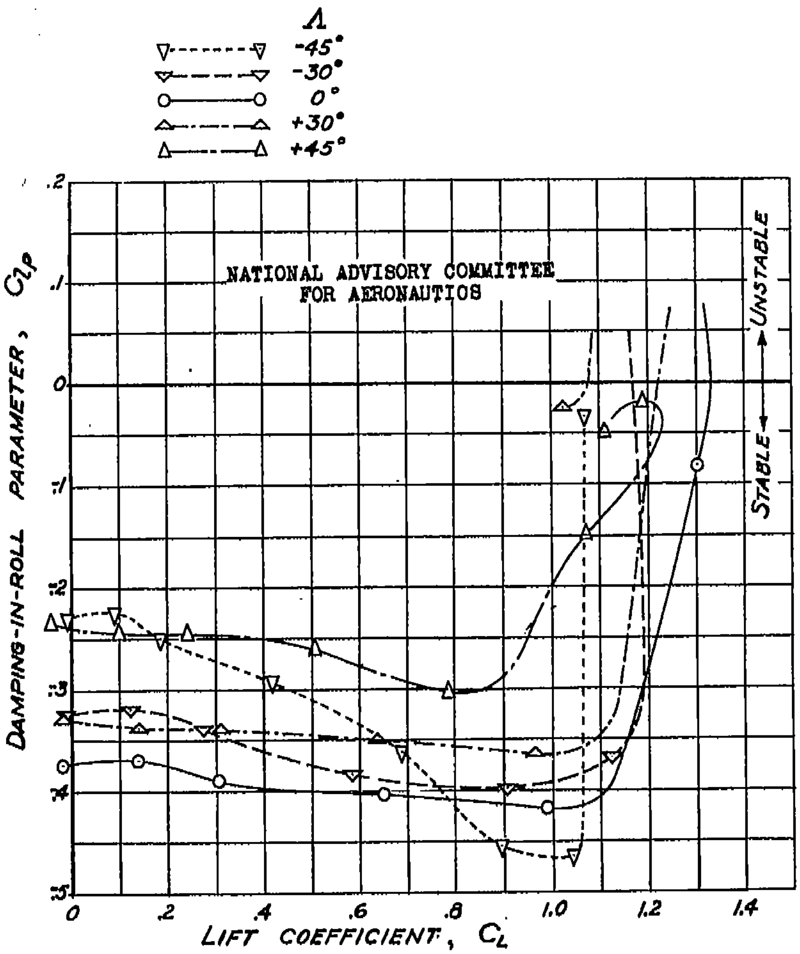

FIGURE 6.– EFFECT OF SWEEP ON THE VARIATION OF DAMPING-IN-ROLL PARAMETER WITH LIFT COEFFICIENT. PLAIN WINGS.

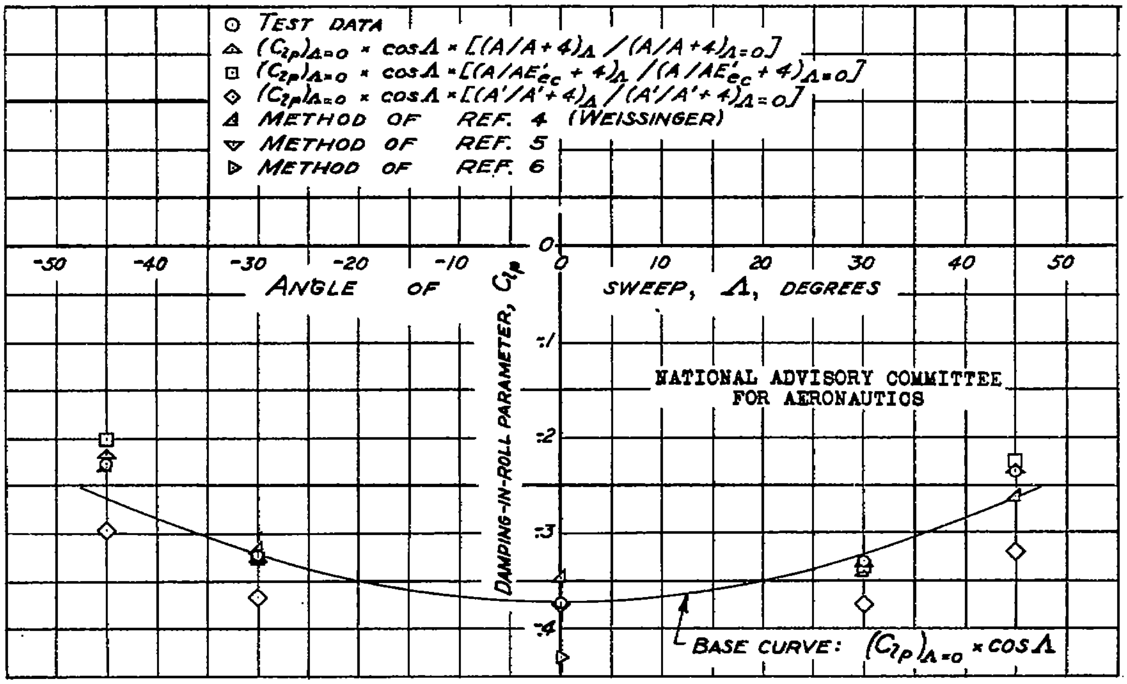

FIGURE 7.– COMPARISON BETWEEN THEORETICALLY AND EXPERIMENTALLY DETERMINED EFFECTS OF SWEEP ON THE DAMPING-IN-ROLL PARAMETER AT ZERO LIFT. PLAIN WINGS.

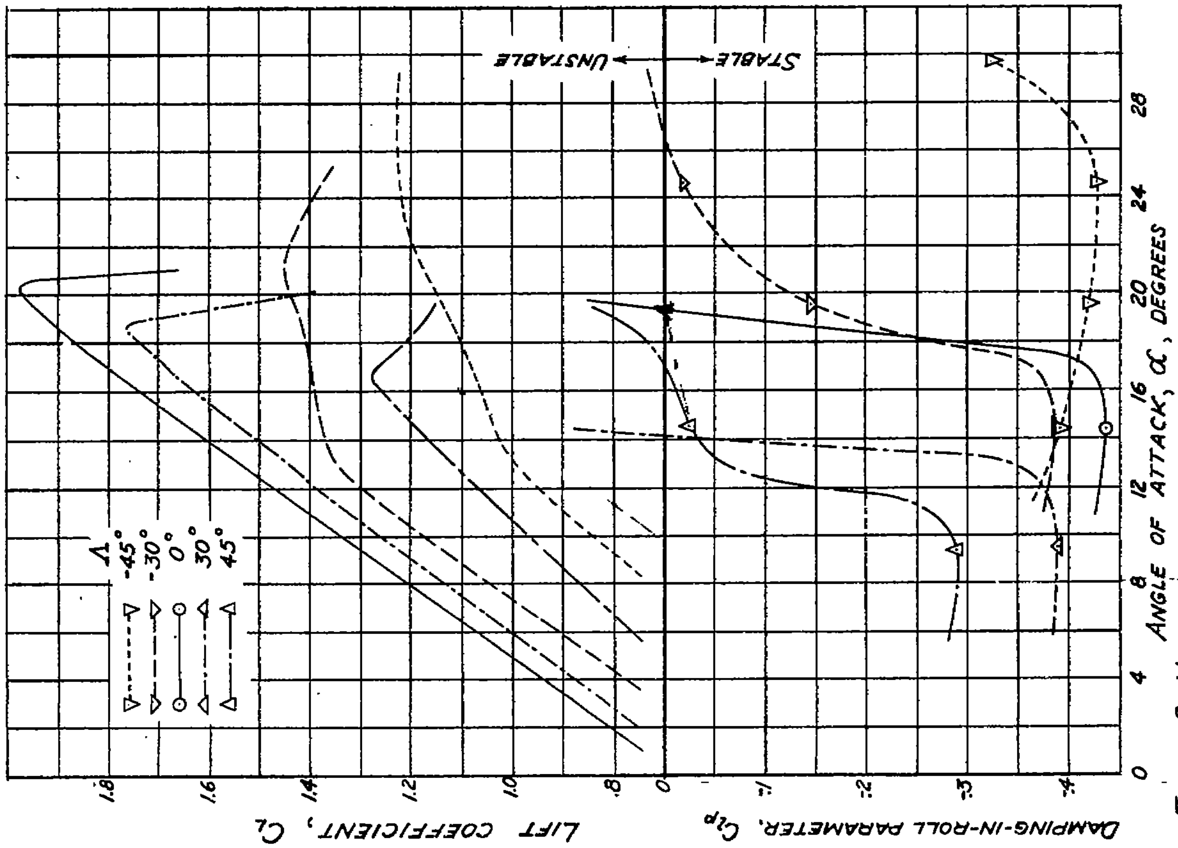

FIGURE 8.– VARIATION WITH ANGLE OF ATTACK OF DAMPING-IN-ROLL PARAMETER AND LIFT COEFFICIENT. FLAPPED WINGS.

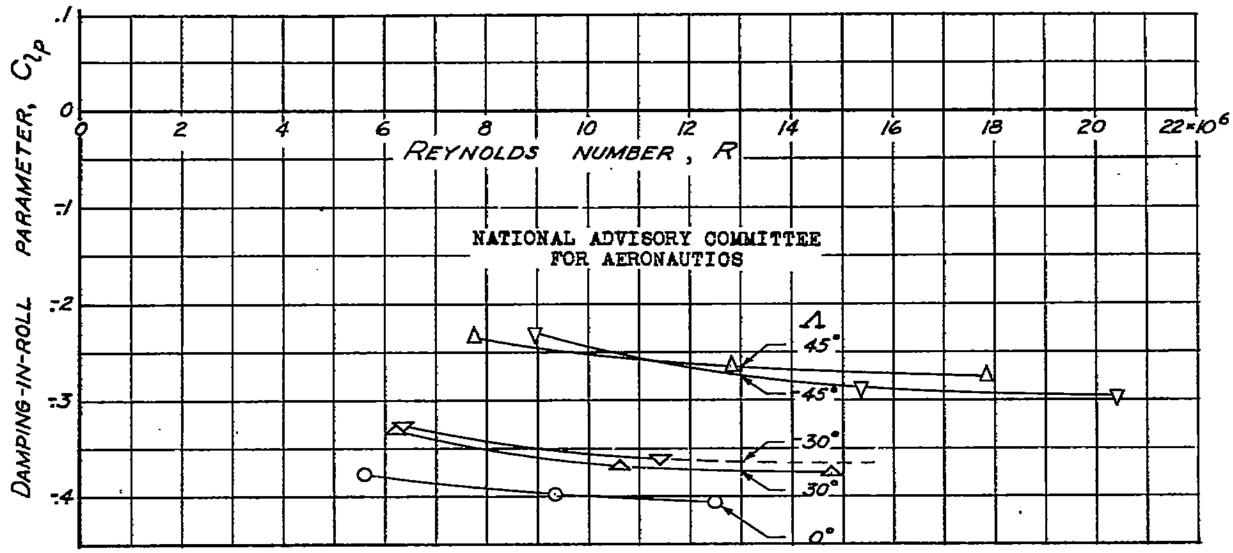

FIGURE 9.– EFFECTS OF SWEEP ON THE VARIATION OF DAMPING-IN-ROLL PARAMETER WITH REYNOLDS NUMBER FOR THE PLAIN WINGS AT ZERO LIFT.

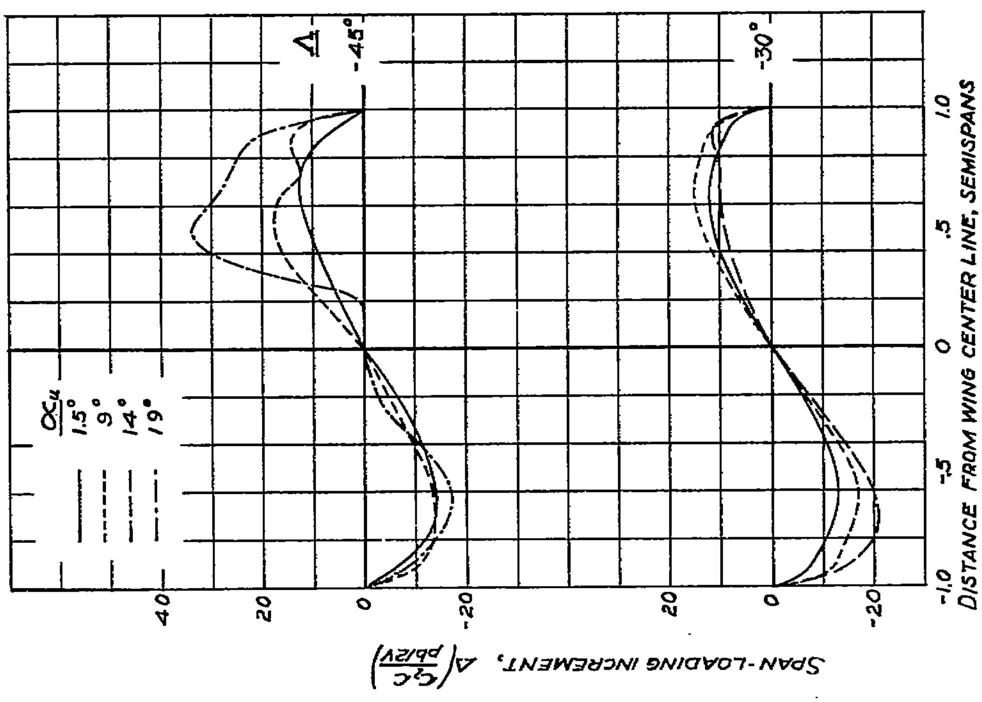

(a) 45° AND 30° SWEPTFORWARD WINGS.

FIGURE 10.– EFFECT OF ANGLE OF ATTACK ON THE SPAN-LOADING INCREMENT GENERATED IN STEADY ROLL FOR THE PLAIN WINGS.

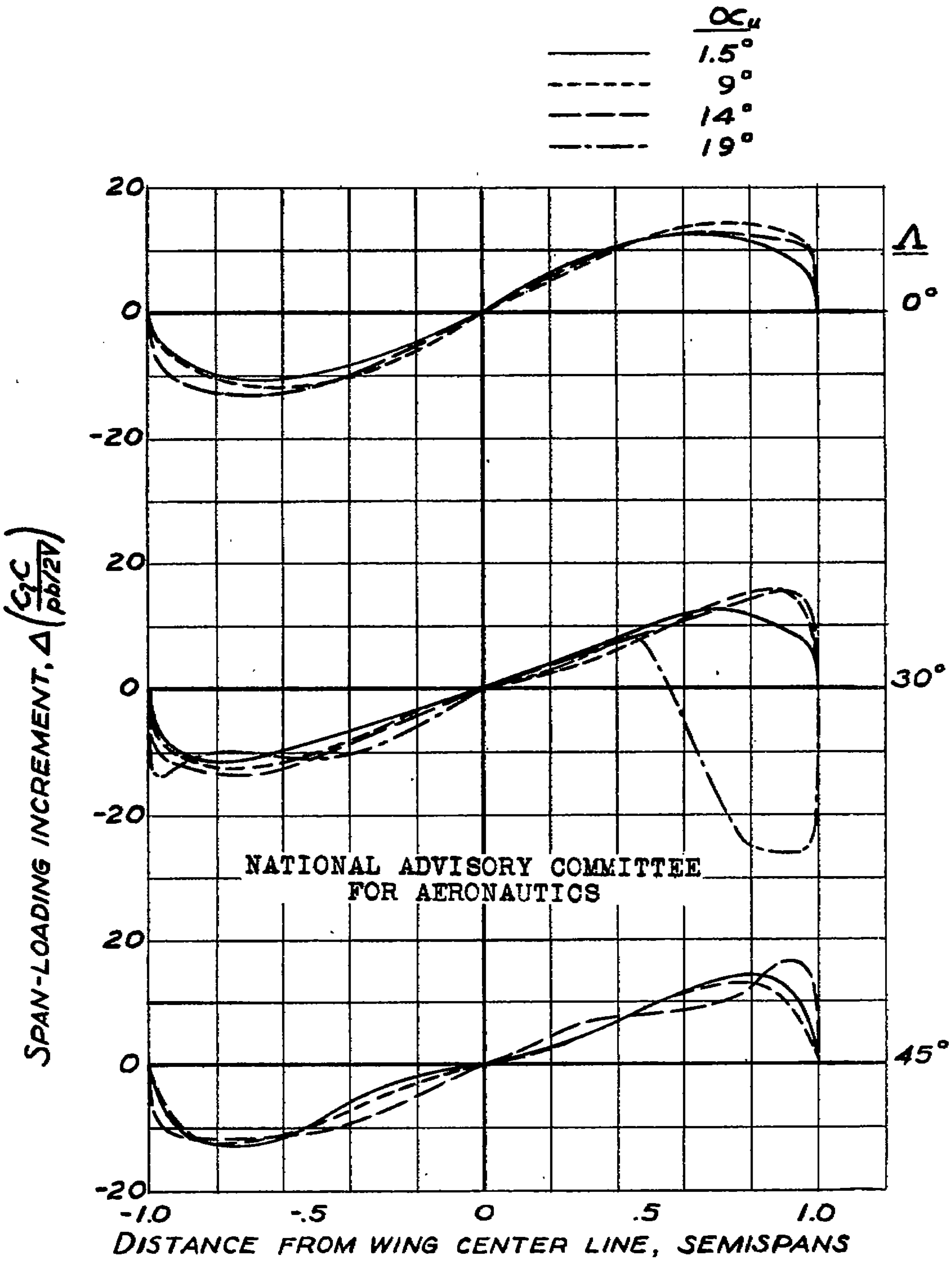

(b) 0°, 30°, AND 45° SWEPT-BACK WINGS.

FIGURE 10.–CONCLUDED.

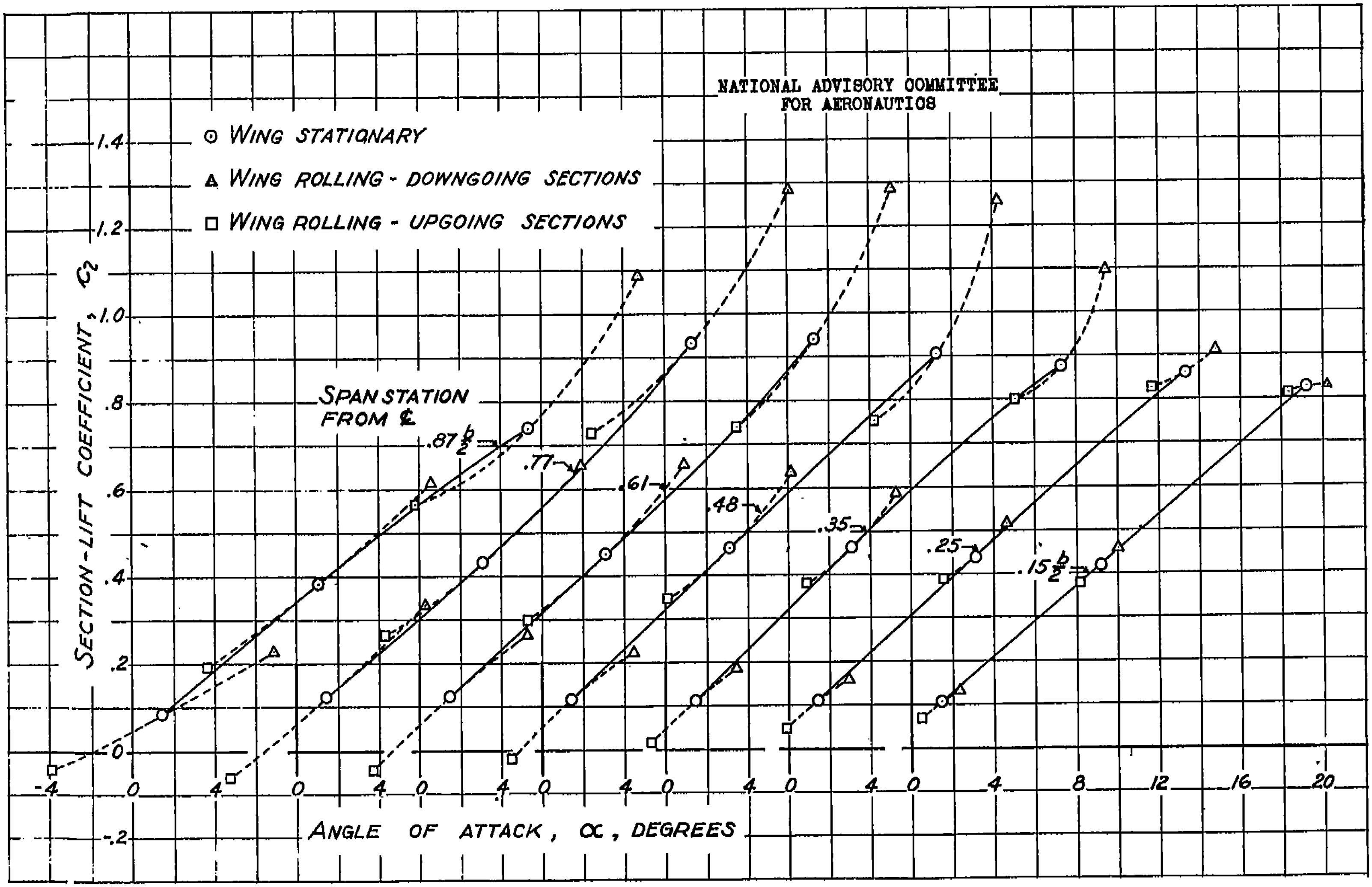

(a) 45° SWEPT-FORWARD WING.

FIGURE 11.– VARIATION OF SECTION-LIFT COEFFICIENT WITH ANGLE OF ATTACK FOR THE PLAIN WINGS STATIONARY AND IN STEADY ROLL AT 0.11 pb/2V.

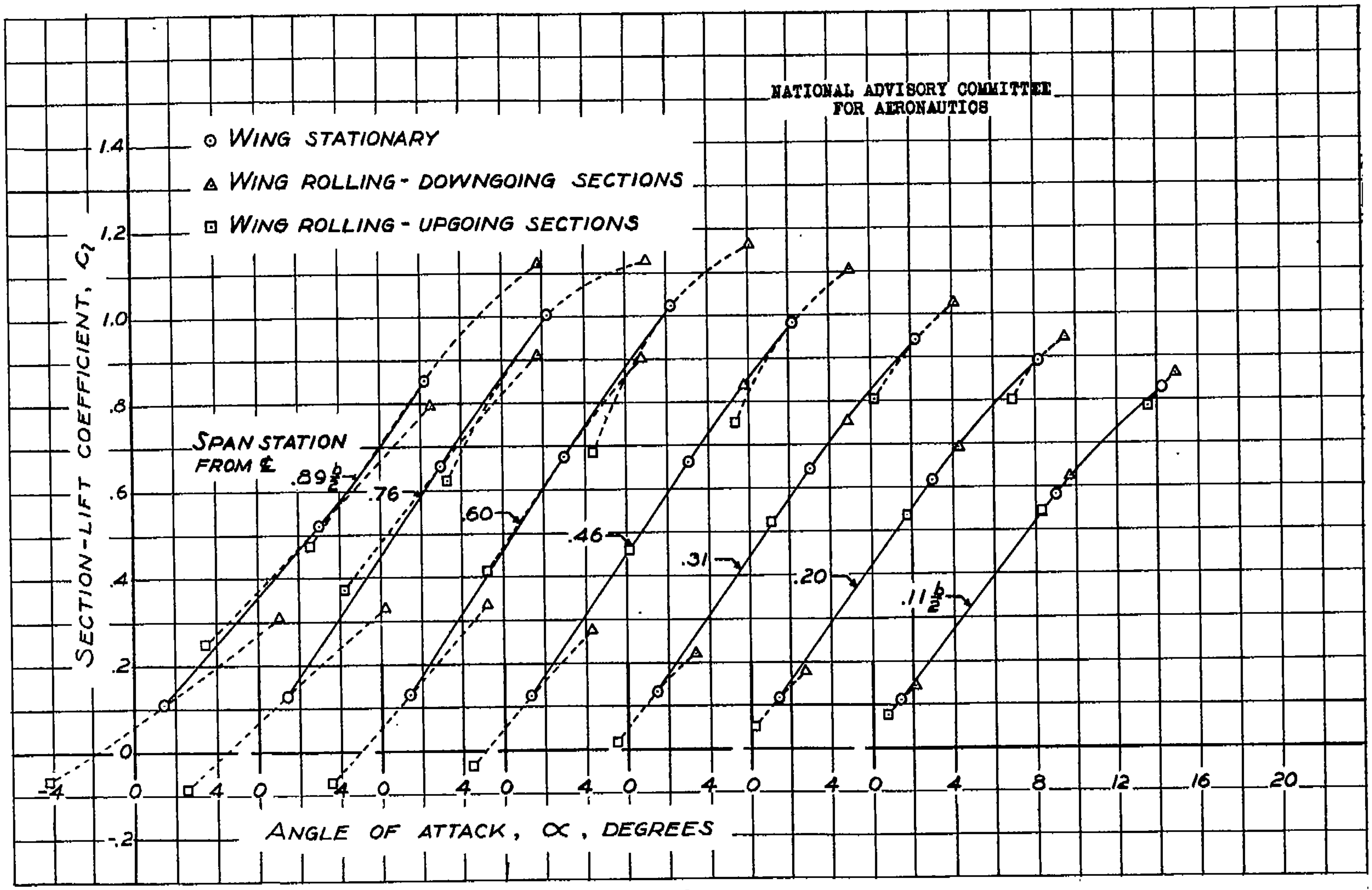

(b) 30° SWEPT-FORWARD WING.

FIGURE 11.- CONTINUED.

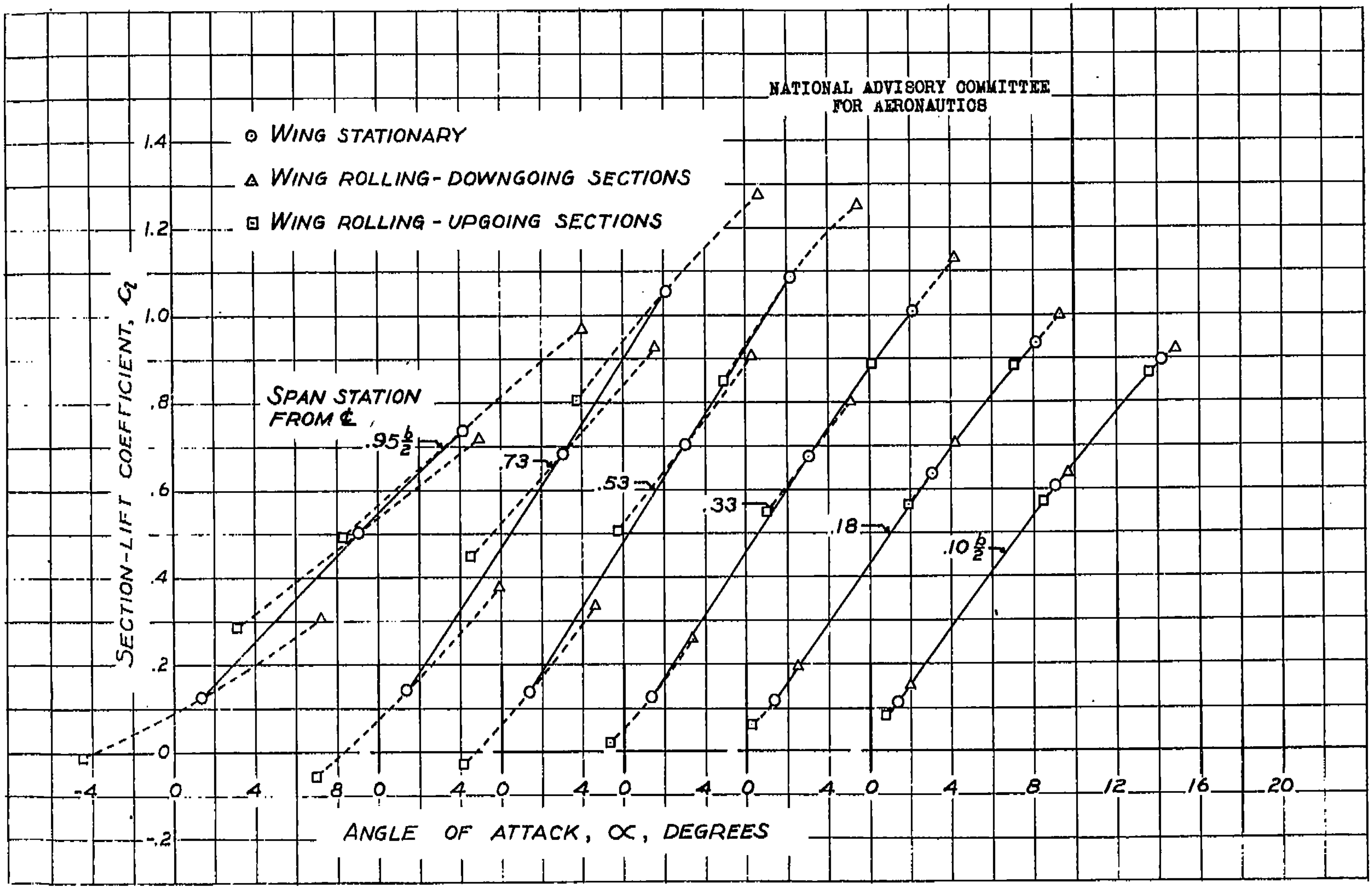

(c) 0° SWEPT WING.

FIGURE 11.– CONTINUED.

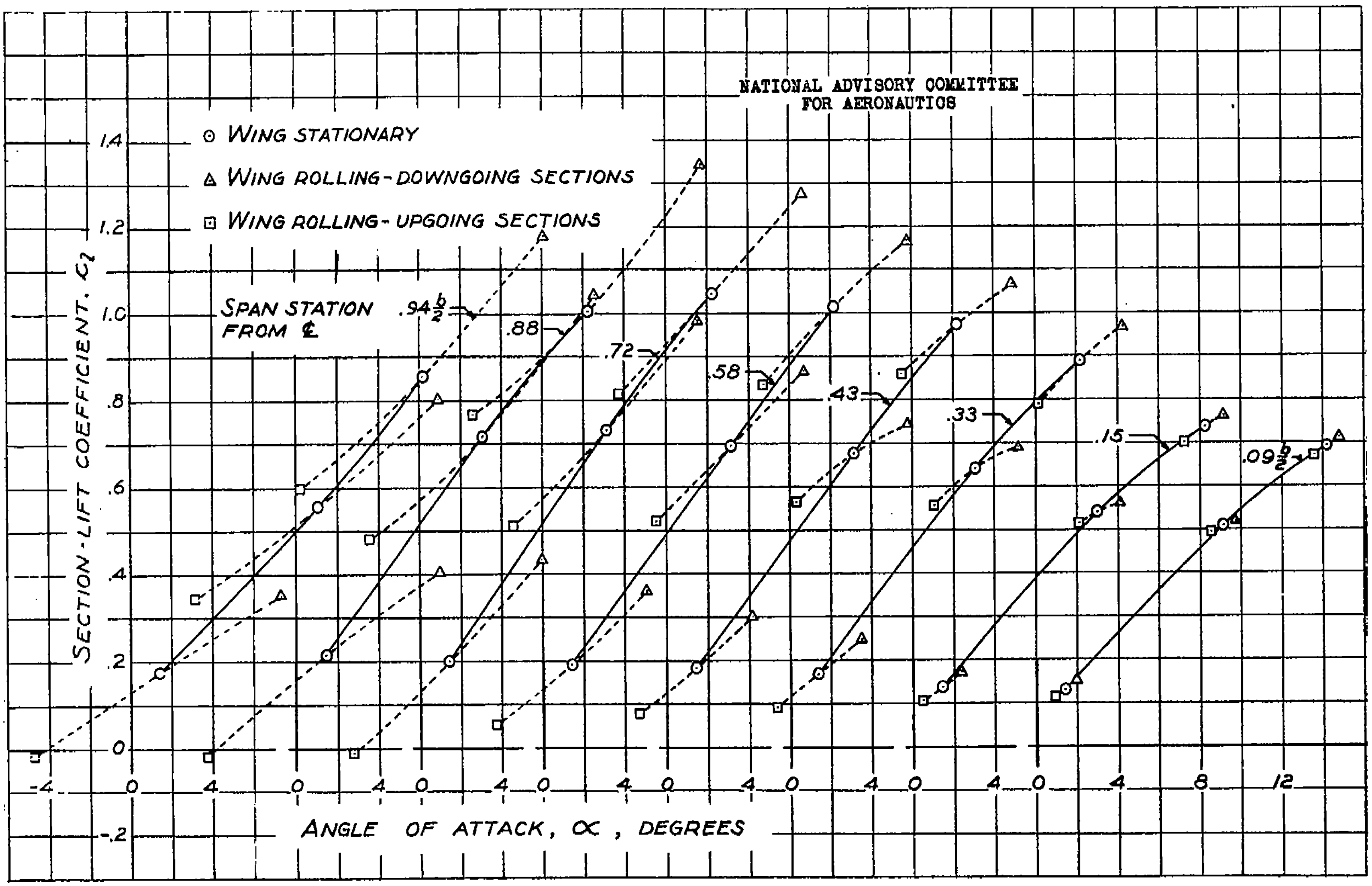

(d) 30° SWEPT-BACK WING.

FIGURE 11.- CONTINUED.

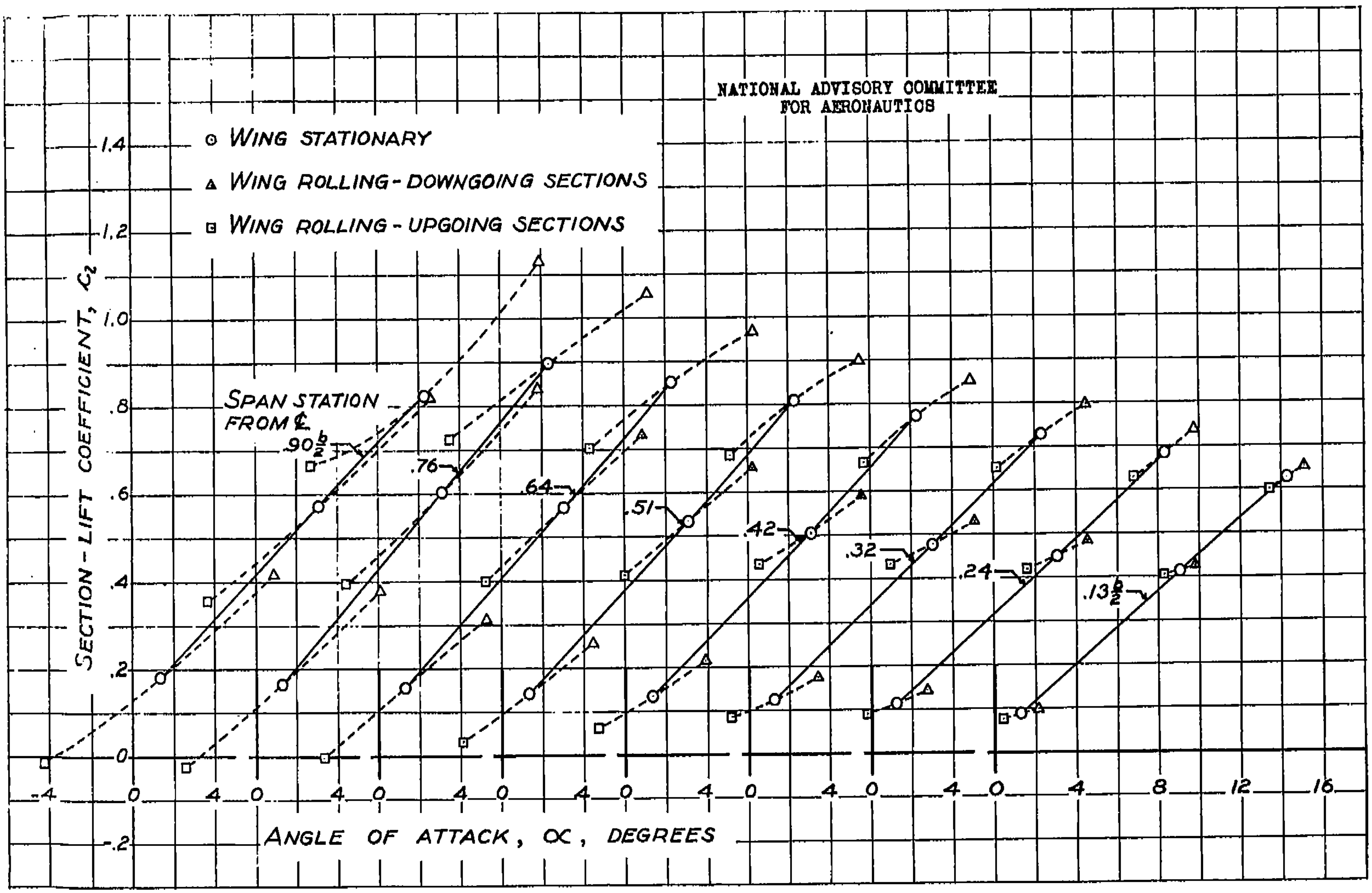

(e) 45° SWEPT-BACK WING.

FIGURE 11.- CONCLUDED.

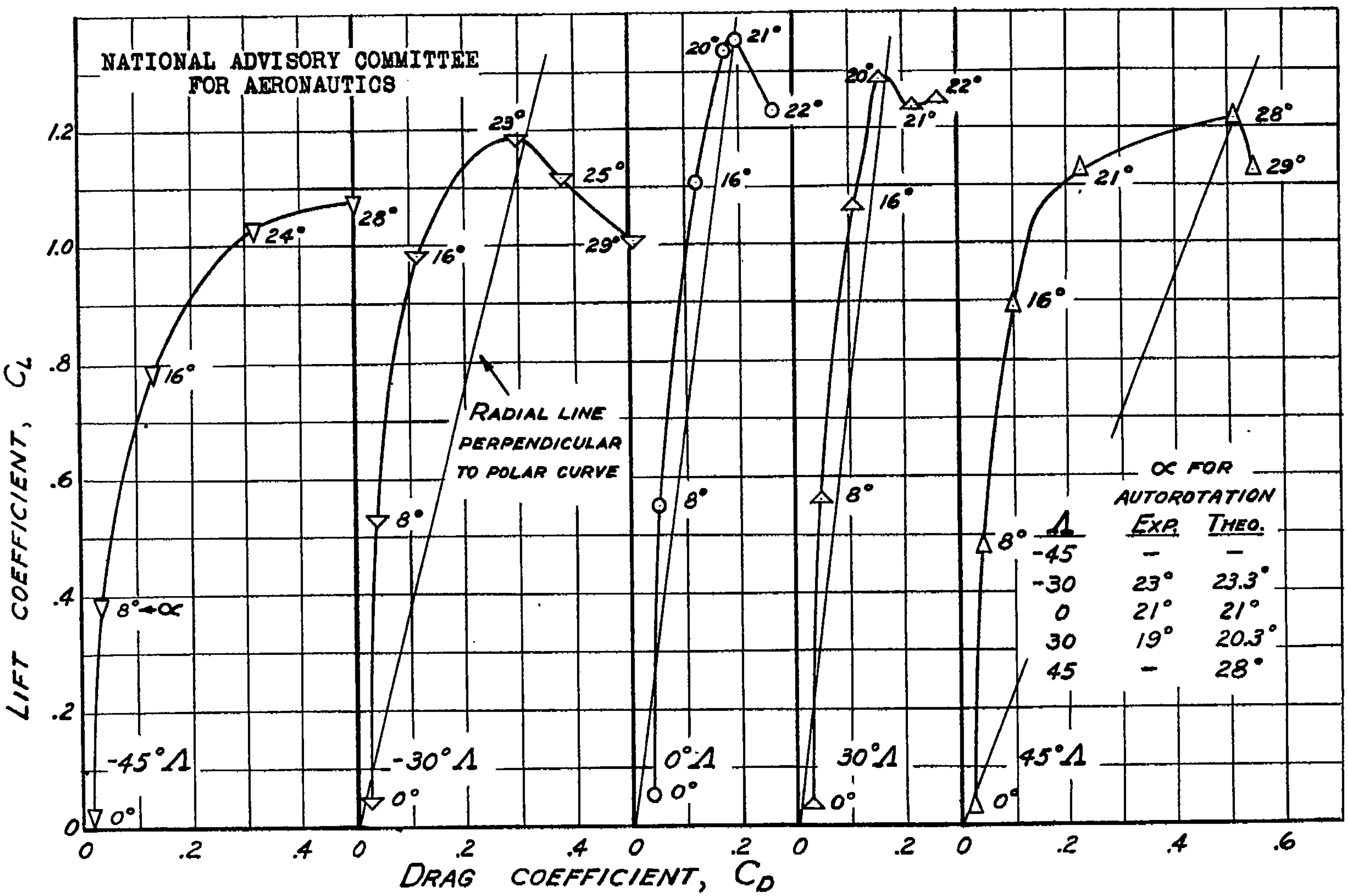

FIGURE 12.- COMPARISON OF AUTOROTATIONAL CHARACTERISTICS OF THE PLAIN WINGS AS DETERMINED EXPERIMENTALLY AND THEORETICALLY.